37th Wright Brothers Lecture*

High-Lift Aerodynamics

A. M. O. Smith
McDonnell Douglas Corporation, Long Beach, Calif.

Nomenclature

c = chord
c_{d_p} = section profile drag coefficient
c_f = local skin-friction coefficient $\tau_w/(1/2)\rho u_e^2$
c_ℓ = section lift coefficient
C_L = lift coefficient
C_p = conventional pressure coefficient $(p-p_\infty)/(1/2)\rho u_\infty^2$
C_p^* = pressure coefficient when local flow is sonic
$\bar{C}_p$ = canonical pressure coefficient $(p-p_o)/(1/2)\rho u_o^2$
C_Q = suction quantity coefficient $Q/u_o x$
C_μ = blowing momentum coefficient $(2u_j^2 t/u_\infty^2 c)$, incompressible flow
$C_{\mu\theta}$ = blowing momentum coefficient referred to momentum thickness of the boundary layer at blowing location, $u_j^2 t/u_e^2\theta$, incompressible flow
f = chord fraction, see Eq. (5.1)
H = shape factor of the boundary layer, δ^*/θ
ℓ = plate length
L = lift
m = exponent in $\bar{C}_p = x^m$ flows, also lift magnification factor (5.1)
M = Mach number
p = pressure
q = dynamic pressure
Q = flow rate
R = Reynolds number ($= u_o x/\nu$ in Stratford flows)
R_θ = Reynolds number based on momentum thickness $u_e\theta/\nu$
S = Stratford's separation constant (4.10); also peripheral distance around a body or wing area
t = blowing slot gap, also thickness ratio of a body
u = velocity in x-direction
u_o = initial velocity at start of deceleration in canonical and Stratford flows
v = velocity normal to the wall
V = a general velocity
x = length in flow direction, or around surface of a body measured from stagnation point if used in connection with boundary-layer flow

Presented as Paper 74-939 at the AIAA 6th Aircraft Design, Flight Test and Operations Meeting, Los Angeles, Calif., August 12-14, 1974; submitted August 14, 1974; revision received December 27, 1974.

Index categories: Aircraft Aerodynamics (including Component Aerodynamics); Boundary Layers and Convective Heat Transfer—Turbulent; Subsonic and Transonic Flow.

A. M. O. Smith, Chief Aerodynamics Engineer for Research at Douglas Aircraft Company, Long Beach, Calif., was born in Columbia, Mo. on July 2, 1911. He majored in Mechanical and Aeronautical Engineering at the California Institute of Technology, receiving the M.S. degree in both fields. After graduation in 1938, he joined Douglas as Assistant Chief Aerodynamicist. During this period, he worked on aerodynamic and preliminary design problems of the DC-5; SBD dive bomber; and the A-20, DB-7, and B-26 attack bombers. He had prime responsibility for detailed aerodynamic design of the B-26.

Because of earlier work with rockets at Caltech, he was asked by Gen. H. H. Arnold to organize and head the Engineering Department of Aerojet as their first Chief Engineer, on leave of absence from Douglas, in 1942-1944. After expanding the department from 6 to more than 400 and seeing the Company into production on JATO units, he returned to Douglas and Aerodynamics. There he handled aerodynamics of the D-558-1 Skystreak and the F4D-1 Skyray, both of which held world speed records.

In 1948 he moved into the research aspect of aerodynamics. Since then he has developed powerful methods of calculating potential and boundary-layer flows, culminating in a book co-authored with T. Cebeci entitled, *Analysis of Turbulent Boundary Layers*. He has published over 50 papers.

For his work at Aerojet, he received the Robert H. Goddard Award of the American Rocket Society. For his early rocket work at Caltech, he is commemorated in bronze at the NASA Jet Propulsion Laboratory. In 1970, he received the F. W. (Casey) Baldwin Award of the CASI, which is in commemoration of the first Canadian to fly an airplane. He is a Fellow of the AIAA.

Presented as Paper 74-939 at the AIAA 6th Aircraft Design, Flight Test and Operations Meeting, Los Angeles, Calif., August 12-14, 1974; submitted August 14, 1974; revision received December 27, 1974.

Index categories: Aircraft Aerodynamics (including Component Aerodynamics) Boundary Layers and Convective Heat Transfer—Turbulent; Subsonic and Transonic Flow.

*Note: The 36th Wright Brothers Lecture by Herman Schlichting was published in the April 1974 *AIAA Journal* but was incorrectly identified as the 37th Lecture.

Greek

α = angle of attack
δ = flap deflection
δ^* = displacement thickness of the boundary layer
θ = momentum thickness of the boundary layer
ν = kinematic viscosity
ρ = mass density
τ = shear stress
ψ = stream function

Subscripts

e = edge conditions
j = jet
ℓ = lower
o = reference conditions, as in Stratford flows
u = upper
w = at the wall
∞ = reference condition at infinity

1. Introduction and Purpose

WHEN I first began work for the Douglas Aircraft Company in 1938, Donald W. Douglas, Jr., was in school. Several times, in connection with his studies, he came to me for help with aerodynamic homework problems, so that we got to know each other. Years later he gave me a 25-year service pin and asked me what I was doing. For once I was quick-witted and answered "still trying to understand aerodynamics."

That is the primary purpose of my lecture—the understanding of one aspect of aerodynamics. It is not a "how to do it" lecture, but rather one concerned with "whys" and principles. Since I am in research, I am not directly involved with the down-to-earth design problems of aerodynamic hardware, but instead am in a position of giving help to others. That reminds me of the definition of a mathematician I once heard. A mathematician is one who can tell you all about how to solve a problem but cannot actually do it himself.

It was my privilege as a graduate student at Caltech to listen to the brilliant beginnings of this series, by B. Melville Jones in 1937. It is a great honor, a privilege, and a difficult challenge to follow him and his many illustrious successors. In his introduction he said "...I am instructed that the Wright Brothers' Lecture should deal with subjects upon which the lecturer is engaged at the time, rather than with a general survey of some wide branch of aeronautical knowledge." To a great extent, that is my plan; the central interest will be subjects with which I have been closely associated.

Because I have been in the aeronautical field for some time now, I find it interesting to look back at the state of aeronautical knowlege when I was in school in the 1930's. I think you will see, as I proceed, that while the problems are far from being completely solved, our capabilities have advanced tremendously. My first problem of substance was my M.S. thesis project. It was to perform tests on a powered Boundary-Layer-Control Model in the GALCIT Ten-Foot Wind Tunnel. Figure 1 is a drawing of the model.

The project was inspired by German work of the time. In the design of the wing, the philosophy—so far as I knew—was as simple as this: 1) select conventional airfoils of the time for the wing, 2) put a slot (square edged) somewhere in the upper surface of the wing (70% chord seemed as good as anything), and 3) suck air and see what happened. There was insufficient knowledge of boundary-layer flow to do anything much more sophisticated. At the end of the tests, the writer had a vague uneasiness that there should be some more scientific approach to the problem of design. That is the way it was in a leading school that was under the leadership of the eminent von Karman and Clark B. Millikan.

At that time, Pohlhausen's approximate method of calculating general laminar flows was a great new development. Only the most rudimentary method was available for estimating turbulent flows in general pressure gradients, for

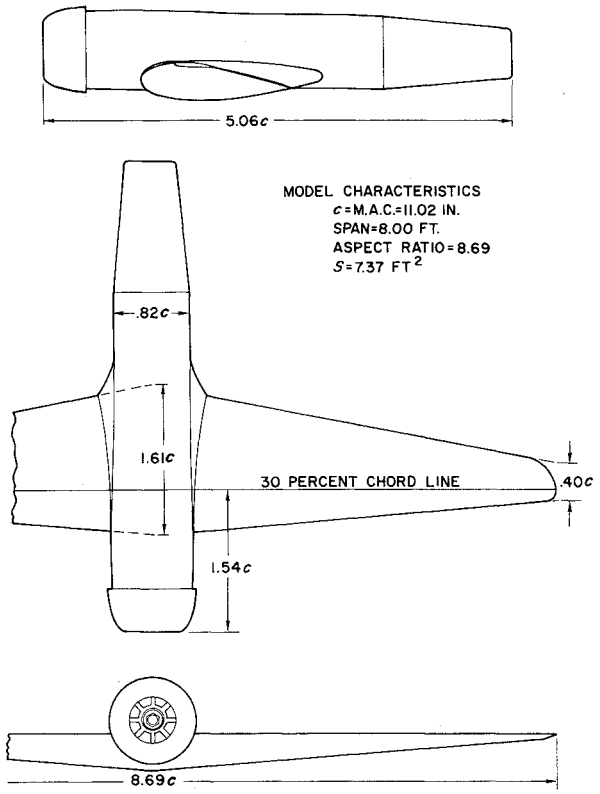

Fig. 1 GALCIT boundary-layer-control wind-tunnel model.

example, over an airfoil surface. The only convenient methods for analyzing inviscid flow about an airfoil were those of thin-airfoil theory and the flow about certain simple conformally mappable sections. Although Theodorsen's method had been developed, it was too tedious for practical use. To calculate the pressure distribution about an arbitrary airfoil amounted almost to a "stunt." Furthermore, all these examples were for single airfoils. Essentially nothing could be done for slotted airfoils. Hence it is no wonder that, in effect, people just drew up a shape by eye and tested it. Performance of airfoils was correlated in terms of certain obvious geometric parameters: camber, position of maximum camber, thickness, etc.

Transition as an explicit phenomenon in the development of a boundary layer was only vaguely recognized. For instance, at the GALCIT tunnel, surely as progressive as any, tests were often made on models of commercial and military airplanes to learn the effect of Reynolds number on drag. Drag coefficients were measured at a series of tunnel speeds. Results were plotted on a log scale and then generally extrapolated by a straight-line extension to full scale. The curve usually had a downward slope with Reynolds number, but not always. Even when the slope was positive, the line would be extended the same way; the effect was dismissed as a "poor Reynolds number extrapolation." Now we know that the model must have been in the rapidly varying transition region, which must surely be left long before full-scale Reynolds numbers are reached. Fixing transition was essentially unheard of. B. Melville Jones, of course, greatly increased our awareness of the transition phenomenon.

2. Some History

Because, unlike the birth of Venus, new ideas do not burst forth fully matured or fully recognized, or even in one place, authoritative establishment of history is difficult. We know better than to attempt it here. Nevertheless, some review of highlights seems desirable.

In a search of the older literature, one of the strongest impressions gained is that in a sense there is "nothing new under

the sun." Nearly all of the basic principles for influencing a flow to develop high lift have been known from the very early days of the airplane. The defects in knowledge were two: first, although what to do may have been known, the reasons for doing it were only dimly understood; second, quantitative analysis of a flow could rarely be accomplished.

Prandtl[1] had already conceived and demonstrated the principles of suction boundary-layer control in 1904, and by 1913, according to Weyl,[2] the notion of blowing to control the boundary layer had been advanced. One concept the author believes to be new is that of the jet flap, which seems to have been conceived and developed in the 1950's. Hagerdorn and Ruden[3] tested forms of the jet flap in 1938, but they did not understand what they were finding.

The ancestry of flaps can be traced back to the early days of flying. British R&M No. 110, dated 1914[4] contains one section entitled, "Experiments on an Aerofoil Having a Hinged Rear Portion." Figure 2 shows the shape tested. A large number of flap settings were examined. According to Weyl,[2] variable camber had been used even earlier. The LeBlon monoplane had a variable-camber wing formed by an adjustable part of the trailing edge. It was exhibited at the London Olympia Show in March, 1910.

The idea of slats and the knowledge of the effectiveness of slots are nearly as old. In an important lecture given before the British Royal Aeronautical Society on February 17, 1921, Handley Page[5] described ten years of work on the development of airfoils that had slots. His work dealt not only with a single slot or slat but also with multiple slots. Figure 3,[6] shows one of his models, which by current standards would be considered a relatively modern configuration. Page 425 of Ref. 7 shows a good photograph of a 1920 airplane fitted out with slats.

Later in this paper, the author attempts to prove that an airfoil having $n+1$ elements can develop more lift than one having n elements. Handley Page investigated this problem, up through 8 elements.[5] Figure 4 shows one of his extreme airfoils, a very highly modified RAF 19 section, positioned at the angle for maximum lift.

Figure 5 shows lift coefficient vs angle of attack for the experimental airfoil as it was modified from one to eight elements. It generally shows that the greater the number of elements the greater the lift; and it seems to confirm the author's deduction, which was made three years ago, quite in ignorance of these tests. The seven-element airfoil reached a lift coefficient of 3.92. Tests were made at a chord Reynolds number of about 250,000 on a wing of 6-in. chord and 36-in. span.

Handley Page appears to have followed an empirical approach in his efforts. Concurrently Lachmann[7] at Göttingen was studying the problem theoretically. Lachmann used conformal-transformation methods and represented a slat by vor-

Fig. 2 RAF 9 airfoil with a 0.385c plain flap tested in 1912-1913.

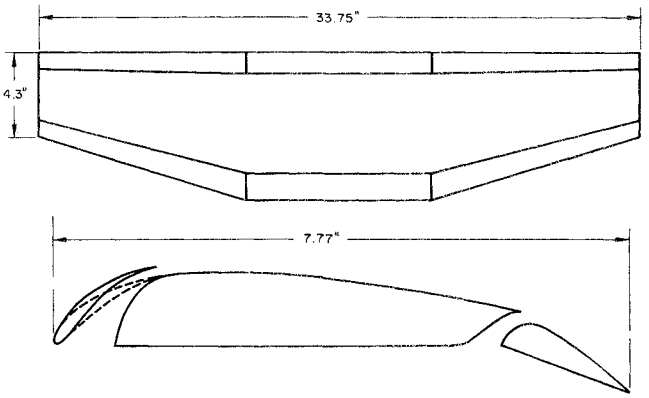

Fig. 3 A wing tested by Handley Page as part of his effort at developing slots and slats.

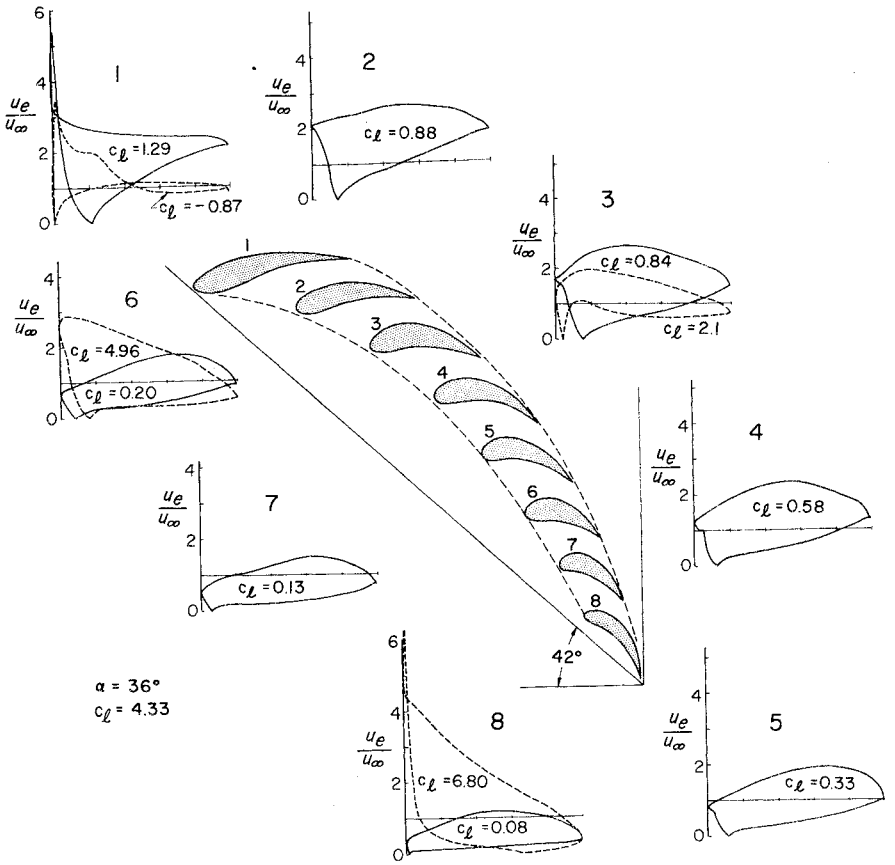

Fig. 4 Handley Page's eight-element airfoil modified from an RAF 19 section. The model is at 42° angle of attack, the angle for maximum lift. Pressure distributions are theoretical. They were made at $\alpha = 36°$ to correspond to local angle of attack of the $AR = 6$ wind tunnel model. Theoretical c_ℓ of ensemble is 4.33.

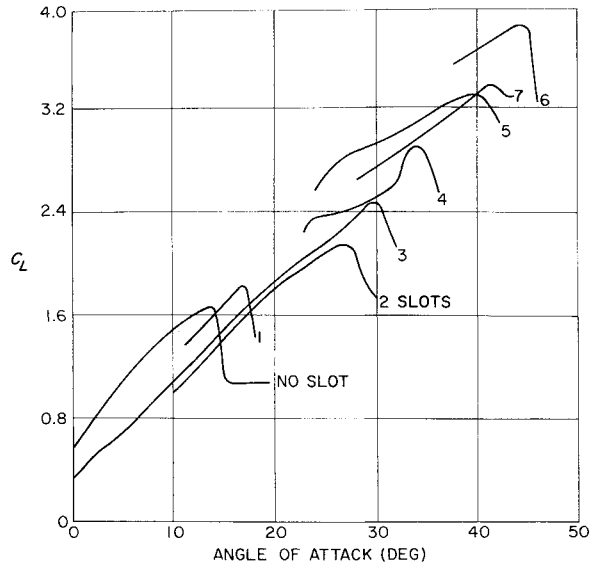

Fig. 5 C_L vs α data for the RAF 19 broken up into different numbers of elements, as indicated by number of slots.

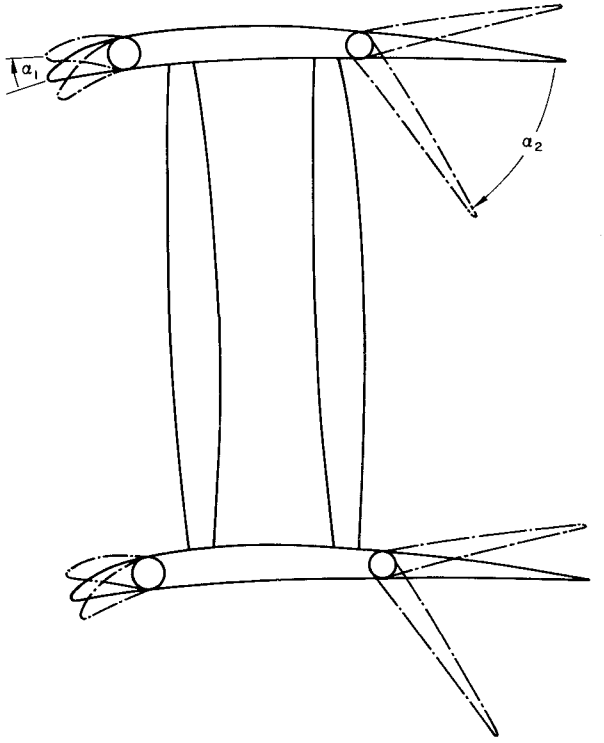

Fig. 6 Variable camber Albatross Biplane[9] model, showing approximate range of flap angles tested.

tices in front of a circular cylinder. His work established the gross features and interaction effects for a slat and the main airfoil. Later, Lachmann and Handley Page joined forces. Further basic understanding and appreciation of the beneficial effects of a slat was gained by Le Page,[8] who systematically investigated the forces on two airfoils placed in tandem.†

Another work that merits mention is entitled "Model Experiments with Variable Camber Wings," by Harris and Bradfield,[9] which was published in 1920. The report includes both test data and studies of the significance of the results on airplane performance. Figure 6 shows the biplane cellule that was studied.

†Louis Stivers and R.T. Jones of NASA Ames inform me that Chaplygin had done work similar to Lachmann's in 1911 and 1921. See *The Selected Works on Wing Theory* of Sergei A. Chaplygin. English translation available through Garbell Research Foundation.

Speaking of biplanes, history seems to be repeating itself. In the early days, because they were biplanes, they had thin wings. These suffered from leading-edge stall, for which nose droop or slats were a cure. Then we advanced to monoplanes and thicker wings, and the leading-edge problem almost disappeared. Later, when jets and higher speed entered the picture, wings again became thin, and the leading-edge problem returned.

Original flap development was motivated by three desired benefits: 1) slower flying speeds, hence shorter takeoff and landing runs; 2) reduction of angle of attack near minimum flying speed; 3) increase of drag, or control of drag, in order to steepen glide angle in approach and reduce floating tendencies. Currently, because of large aircraft noise problems, the emphasis under the third item has changed. We are trying to reduce flap drag in order to reduce thrust requirements and hence the noise.

The split flap was conceived and partly developed in the period 1915-1920 as a means of satisfying these desires. Klemin, Schrenk, and Etienne Royer[2] are important contributors to its development. Orville Wright and J. M. H. Jacobs obtained a basic patent on the subject in 1924, after they filed it in 1921. Their discussion in the patent gives evidence that they had a good qualitative understanding of the basic flow processes. A reproduction of one of the drawings from the patent is shown in Fig. 7.

We end this historical survey of mechanical high-lift devices by mentioning the Fowler Flap invented by Harlan D. Fowler[10] in 1927. Because it had extension and a slot, it can be considered to be the first modern high-lift mechanical flap. In early NACA wind-tunnel tests,[11] it developed a maximum lift coefficient of 3.17.

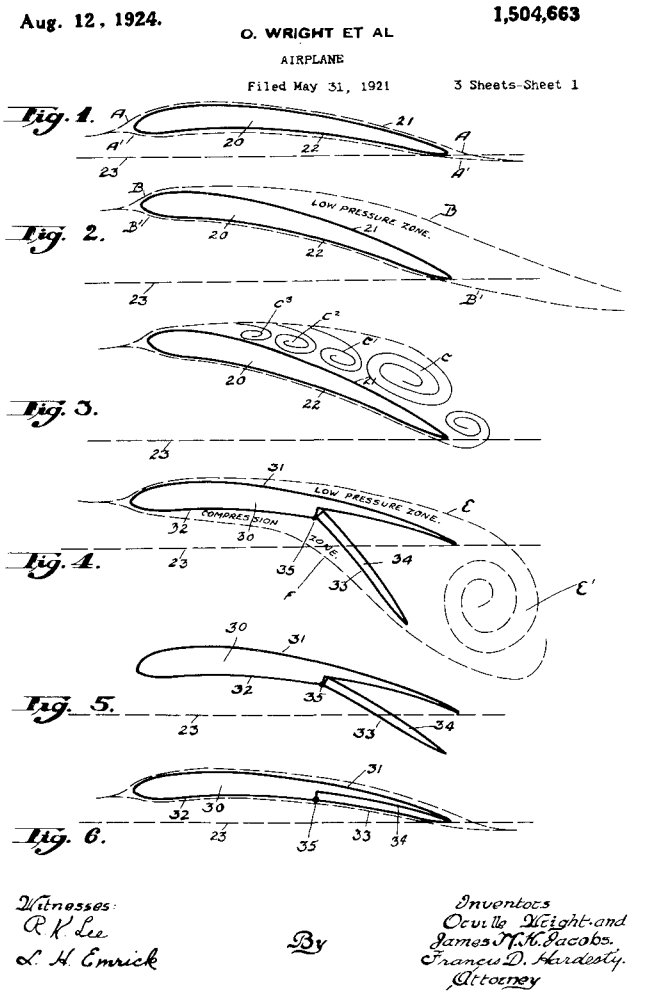

Fig. 7 Sheet 1 of the U.S. Patent 1,504,663, by Orville Wright and J. M. H. Jacobs, illustrating their concept of a split flap.

Powered lift augmentation, as by suction and blowing, received considerable attention in the 1920's but never quite proved to be efficient enough to justify its use in an actual airplane. Betz[2] and Ackeret[7] in Germany were leaders in this line of development.

For those interested in further research into the early history of high-lift work, we mention several references. First is that by Alston,[12] which was a general lecture to the Royal Aeronautical Society in 1934 entitled, "Wing Flaps and Other Devices as Aids in Landing." It surveys the state of knowledge in 1934, but does not particularly deal with earlier history. Those who are especially interested in the history of high-lift devices and the origin of concepts and applications should see the paper by Weyl,[2] which is a very broad survey—it has 116 references—of the entire subject, with interesting sidelights on the development. As an example of such a sidelight, Weyl notes that in connection with the development of split flaps a French scientist, Lafay, in 1912 observed "that an unsymmetrical roughening of a cylinder which was exposed to an airflow resulted in an aerodynamic force which was directed towards the smooth side across the flow (lift force)."

The most comprehensive reference examined by the author is a report by A. D. Young,[13] "The Aerodynamic Characteristics of Flaps." It deals with the aerodynamic characteristics—lift, drag, moment, etc.—of all types of flaps. Its extensive bibliography covers all aspects, including general reviews, history, theory, and investigations of the various types of devices. In all, 138 references are given. The paper is certainly not obsolete, although it was published in 1953.

A paper that amounts to an updating of Alston's[12] is one by Duddy,[14] which was also presented to the Royal Aeronautical Society. It compares and evaluates various types of flaps, and analyzes their benefits in terms of landing and takeoff performance. Effects of sweep are included.

A useful historical summary of the gradual improvement of gross lift coefficients is shown in Fig. 8, which is due to Cleveland.[15] From about 1935 to 1965—a period of 30 years—we have advanced from coefficients of roughly 2 to roughly 3 on important service-type airplanes. By 1995 will we have advanced to 4?

3. Some Lift Limits

3.1 Limits in Potential Flow

Just as ideal-cycle limits are useful in thermodynamics, so are the theoretical limits of lift useful in aerodynamics. Knowledge of those limits helps give us a perspective as to where we are now and what may be attainable if we are willing to seek without compromise the maximum possible lift.

First consider the limits of c_ℓ in inviscid flow, where separation will not occur. Consider the classical circulatory flow about a circle shown in Fig. 9. Two different levels of circulation are shown; that in Fig. 9b is of the greatest interest, for there the circulation is so strong that front and rear stagnation points coincide. Greater circulation moves the stagnation point off the body. Although that is entirely possible—a Flettner Rotor generates such flows—it is not a realistic analog for an airfoil, which in general has two stagnation points, both on its surface. If the reference chord is taken as the diameter of the circle, it is easily shown that flow b of Fig. 9 represents a lift coefficient,

$$c_\ell = 4\pi \tag{3.1}$$

where the reference length is the diameter.

Now let us consider mean lines. We shall consider only circular arcs, because they are easily obtained from Joukowski's transformation for flow about a circle. In view of the ever present specter of separation, it is an undue refinement to consider either the effects of thickness or the effects of other kinds of mean lines. Three possible circular-arc mean lines, A, B, and C are shown in Fig. 10. A fourth or limiting case is just a straight line. According to Joukowski airfoil theory, for any of those circular-arc mean lines, regardless of degree of camber,

$$L = \pi\rho V_\infty^2 c[\sin(\alpha+\beta)]/\cos\beta \tag{3.2}$$

In that equation, c is the length between the ends of the arcs, α is the angle of attack, and β is a measure of the camber as shown in Fig. 10. For arcs A and B, c is indeed the chord as conventionally defined. But for arc C, the chord c is not now the longest dimension; the diameter is. In fact, it is evident from the figure that as $\beta \to 90°$, $c \to 0$. Hence, if we define the lift coefficient in terms of the longest dimension, we have [from Eq. (3.2)],

$$c_\ell = 2\pi[\sin(\alpha+\beta)]/\cos\beta \quad (0 \le \beta \le 45°) \tag{3.3}$$

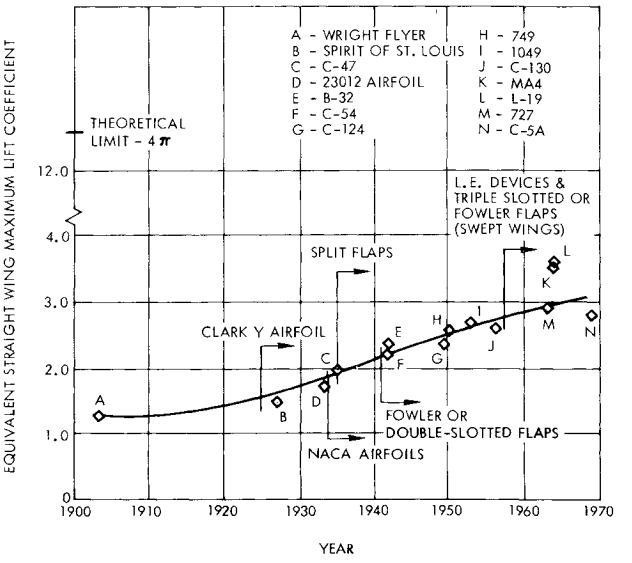

Fig. 8 Growth of maximum lift coefficients for mechanical lift systems as a function of time, according to Ref. 15.

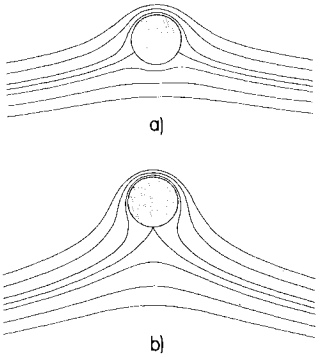

Fig. 9 Flow about a circle with two different degrees of circulation. a) moderate circulation, b) circulation so strong that the two stagnation points coincide.

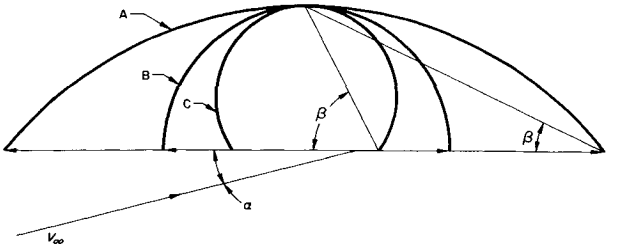

Fig. 10 Three circular-arc mean lines, A, B, C, stemming from the Joukowski transformation.

and

$$c_\ell = 4\pi \sin\beta \sin(\alpha+\beta) \quad (45° \le \beta \le 90°) \tag{3.4}$$

Consider Eq. (3.3) with $\beta = 0$. We have a flat-plate airfoil. Its maximum lift coefficient is 2π at $\alpha = 90°$. A well-known formula applying to symmetrical Joukowski airfoils that accounts for thickness ratio t is

$$c_\ell = 2\pi(1+0.77t)\sin\alpha \tag{3.5}$$

That formula gives a value that is a few percent greater for common values of t.

Next, consider Eqs. (3.3) or (3.4) with $\beta = 45°$. That mean line is a half circle. Maximum lift occurs at $\alpha = 45°$, so that

$$c_{\ell max} = 4\pi/(2)^{1/2} \quad (\beta = 45°) \tag{3.6}$$

Finally consider Eq. (3.4). The maximum occurs when $\beta = 90°$ and $\alpha = 0°$, which gives

$$c_{\ell max} = 4\pi \tag{3.7}$$

The limiting mean line is a complete circle. For airfoils with some thickness, there is a definite stagnation point at the nose and another one at the tail. Hence, that limiting mean line brings the two stagnation points together again, and we effectively recover the flow about a circular cylinder, as in Fig. 9b.

The last is an extreme mean line. The half-circle is not so extreme. In fact, modern multielement flap systems at full flap deflection begin to approximate the half-circle mean line (e.g., Fig. 29). The quantity $c_\ell = 4\pi/(2)^{1/2}$ in Eq. (3.6) has a value of nearly 9. Of course, the value of c_ℓ depends on the length used as a reference. If arc length were used instead of conventional chord, as above, the values would not appear to be so high. In fact, for the straight line, half circle, and full circle, the theoretical values would be 6.28, 5.65, and 4.0, respectively.

The mean lines that have been considered approximate flows about airfoils having sharp trailing edges. For them, the Kutta condition sets the circulation to such strength that the rear stagnation point is always at the trailing edge. Such a flow might be called a natural flow. To round out our discussion, we shall mention a case in which there is no sharp trailing edge: the ellipse family. Assume the circulation to be controlled in such a way that the rear stagnation point always remains at the rear end of the x-axis, that is, at the same point as in symmetric nonlifting flow (see Fig. 11). Thwaites[16] proposed airfoils that followed that principle. He used area suction at the rear to eliminate separation. When our condition for the circulation is met, the lift coefficient based on the length of the x-axis becomes exactly

$$c_\ell = 2\pi(1+t)\sin\alpha \tag{3.8}$$

If c_ℓ were based on the length of the y-axis, it would be

$$c_\ell = [2\pi(1+t)/t]\sin\alpha \tag{3.9}$$

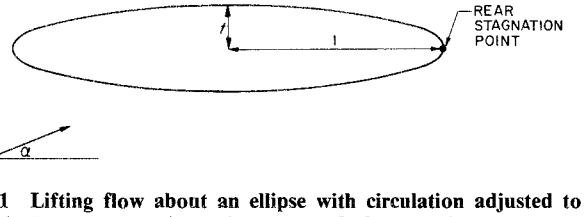

Fig. 11 Lifting flow about an ellipse with circulation adjusted to maintain the rear stagnation point at the end of the x-axis.

Observe that Eq. (3.8) is nearly the same as Eq. (3.5). The circular-cylinder case is represented by $t = 1$, and again we recover $c_\ell = 4\pi$. Equation (3.8) shows that c_ℓ greater than 4π can be exceeded if t is greater than 1, that is, for ellipses that are broadside to the flow. In those cases, we are not using our greatest length as the reference length. We now should use the thickness instead of the length and obtain Eq. (3.9). If Eq. (3.9) is used, $c_{\ell max}$ falls continuously as t increases. Since both formulas give $c_{\ell max} = 4\pi$ for a circle, we once more recover 4π as a limit. That is the limiting value for any single-element airfoil. We know that in a uniform stream $L = \rho V_\infty \Gamma$, where Γ is the circulation. Of course, any airfoil can be mapped from a circle. But the mapping does not change the circulation. Hence, under the restrictions we have imposed, the maximum possible lift for any kind of airfoil is 4π.

Since lift is needed near the ground perhaps more than anywhere else, an interesting subsidiary question is the potential flow limit at the ground. The author knows of no simple definitive answer. However, the Douglas Neumann program was applied to a circle that was brought nearer and nearer to the ground, using the image system. The stagnation point was maintained at the bottom as in Fig. 9b. For zero height off the ground the lift coefficient extrapolates to about 4.49, which is also the value found for the classical problem of a round cylinder lying on a streambed. Ground, therefore, greatly reduces the maximum possible lift. We realize full well that ground effect often increases the lift of real wings.

3.2 Limits of $M_\infty^2 C_L$

High values of C_L cannot be maintained indefinitely as speed is increased, for soon surface pressures less than absolute zero would be indicated. Let us look into the problem briefly, and search especially for the limits of lift rather than of lift coefficient. The usual equation for lift is

$$L = \tfrac{1}{2}\rho_\infty V_\infty^2 C_L S \tag{3.10}$$

An alternate form, one that uses a different expression for dynamic pressure, is

$$L = \tfrac{1}{2}\gamma p_\infty M_\infty^2 C_L S \tag{3.11}$$

With $\gamma = 1.4$, we can rewrite it as

$$L/p_\infty = 0.7(M_\infty^2 C_L)S \tag{3.12}$$

Since C_L is known to be a function of M_∞, the product $M_\infty^2 C_L$ is the quantity that is of real significance, and so we seek to make statements about its value. Observe that for a given value of $M_\infty^2 C_L$ the lift is now proportional to the atmospheric pressure.

A gas cannot be in tension. Hence the limiting suction pressure is a perfect vacuum over the entire upper surface. The limiting pressure on the lower surface is stagnation pressure.

By definition, with $\gamma = 1.4$,

$$C_p = \frac{p - p_\infty}{1/2\rho_\infty V_\infty^2} \equiv \frac{p - p_\infty}{0.7 p_\infty M_\infty^2} \tag{3.13}$$

If the flow is assumed to be isentropic, C_p can be written in the form

$$C_p = \frac{1}{0.7M_\infty^2}\left[\left(\frac{1+0.2M_\infty^2}{1+0.2M^2}\right)^{3.5} - 1\right] \tag{3.14}$$

Before proceeding to the determination of lift limits, it is interesting to pause and consider the limits of C_p values. In high-lift testing, maximum lift is often found to occur when the highest local velocities reach a Mach number of 1.0. The C_p corresponding to that condition will be called C_p^*. If a per-

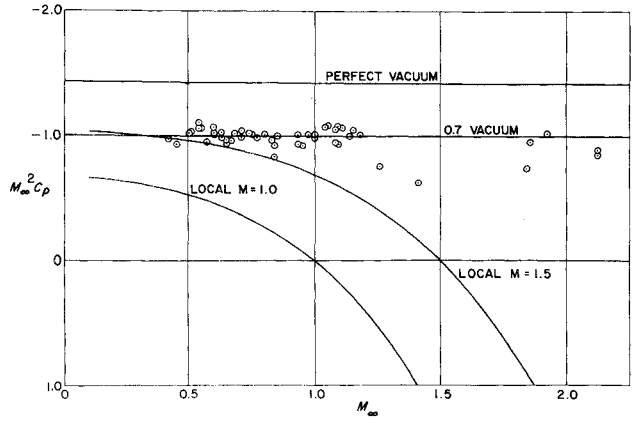

Fig. 12 $M_\infty^2 C_p$ values as a function of Mach number for four conditions. 0.7 vacuum corresponds to $M_\infty^2 C_p = -1$.

Table 1 Limiting values of C_p at low Mach numbers

M_∞	0.10	0.15	0.20	0.30	0.40	0.50
C_p^* (M=1)	-67	-29.3	-16.3	-7	-3.7	-2.1
C_p (perfect vacuum)	-143	-63.6	-35.8	-15.9	-8.9	-5.7
C_p (0.7 vacuum)	-100	-44.5	-25	-11.1	-6.3	-4.0

fect vacuum were reached, we would obtain, according to Eq. (3.13), a value of $M_\infty^2 C_p$ equal to -1.43. Mayer[17] looked for the highest possible negative C_p values in experiment by examining hundreds of NACA test data points from all sorts of tests. He found the remarkable empirical result that the highest experimentally measured values correspond with reasonable accuracy to $M_\infty^2 C_p = -1$. That value corresponds to 0.7 of a vacuum [see Eq. (3.13)]. Figure 12 shows the test data he used to support the finding.

Since much of our interest is in high-lift testing, which is done at low Mach numbers, we convert some of the results from Fig. 12 into C_p form and present them in Table 1.

At low Mach numbers, quite high values of C_p are obtainable before compressibility becomes very important, but at higher Mach numbers the limiting C_p values are not very high. Note, however, that Mayer's data in Fig. 12 do not cover the lower Mach numbers; hence their validity there is not truly established.

The author knows of no theoretical explanation for Mayer's 0.7 vacuum correlation. It does not correspond to a constant local Mach number. By the use of Eq. (3.14), it is easily deduced that $M_\infty^2 C_p = -1$ corresponds to $M_{\text{local}} = 1.43$ at $M_\infty = 0$ and 1.55 at $M_\infty = 0.5$.

Now consider the airfoil problem. If we hold M constant at one value on the upper surface and constant at another value on the lower surface, C_p represents the C_L for each surface. The total C_L is the difference. Hence from Eq. (3.14),

$$M_\infty^2 C_L = \frac{1}{0.7}\left[\left(\frac{1+0.2M_\infty^2}{1+0.2M_\ell^2}\right)^{3.5} - \left(\frac{1+0.2M_\infty^2}{1+0.2M_\mu^2}\right)^{3.5}\right] \tag{3.15}$$

where ℓ and μ denote lower and upper surfaces. A perfect vacuum on the upper surface corresponds to $p_\mu = 0$ or $M_\mu = \infty$. In that case, the second term in Eq. (3.15) is zero. With respect to atmospheric pressure, the load carried by the upper surface when there is a perfect vacuum is [see Eq. (3.13)]

$$M_\infty^2 C_L = 1/0.7 = 1.43, \quad \text{a constant} \tag{3.16}$$

If the entire flow on the lower surface is a stagnation flow, $M_\ell = 0$, and hence with a vacuum on the upper surface we have

$$M_\infty^2 C_L = (1+0.2M_\infty^2)^{3.5}/0.7 \tag{3.17}$$

Equation (3.17) represents the absolute lifting limit. The quantity increases with Mach number because lower-surface pressures can increase with Mach number. Equation (3.17) is optimistic, because isentropic compression is assumed, whereas in reality there surely will be a shock when $M \gg 1$. Table 2 shows values of $M_\infty^2 C_L$ for several flow conditions, including Mayer's $M_\infty^2 C_L = 1$ limit. The maximum value possible in subsonic flight is 2.71, and the contributions from each surface are about equal. If Mayer's value $M_\infty^2 C_p = -1$ is accepted, the limit decreases to 2.28. At $M_\infty = 0.5$, the absolute maximum value is only 1.70 and Mayer's value is 1.27. Those are the limiting values, regardless of the kind of high-lift devices that are used. At $M_\infty = 1.0$ and below, the assumption of isentropic recompression on the lower surface is very good, as is well known. As Mach numbers become large, pressures on the lower side become great, and large values of $M_\infty^2 C_L$ develop—values that exceed 11 at $M_\infty = 2.0$. Mayer considers the case where under-surface pressures in supersonic flight correspond to a normal shock. He gives considerable information on maximum-lift values in supersonic flight, including correlations of theory and experiment. But since our interest is principally in subsonic flight, we shall not discuss his work further.

3.3 Demonstrated Lifting Limits

It is interesting that the question of aerodynamic lifting limits in subsonic flight was posed to the author in 1946 by E. H. Heinemann. The problem was fighter maneuvering—what lift could a wing really develop? All the available flight and wind-tunnel data were examined. The examination included the large supply of German World War II data, which covered tests of a great variety of airplane and missile-type wings. The results were reported in Ref. 18. The study, which was strictly one of observation, concluded that the maximum possible lift was about 1/2 atm. That number corresponds to a value for $M_\infty^2 C_L$ of about 0.7.

Since that time, the design of swept wings has advanced considerably. Now, the highest value of $M_\infty^2 C_L$ seen by the author is 1.20 on a swept wing using an aft-loaded airfoil section with no auxiliary lift devices. The value corresponds to $C_L = 1.26$ at $M_\infty = 0.975$. It was not really a maximum-lift value but, rather, a stopping point in a wind-tunnel test that was determined by strength of the sting support. Hence the value can surely be exceeded. It should be pointed out that this is not a buffet limit, which is usually considerably lower. If one went all out to maximize $M_\infty^2 C_L$, without regard to low-lift performance, much better could surely be done. Leading-edge and trailing-edge devices undoubtedly would raise the limit. Variable-camber wings are currently receiving attention as another possible means of raising the limit.

Some further data related to limiting lift conditions are

Table 2 Maximum-lift limits assuming isentropic compression, and uniform chordwise loading

M_∞	M_{upper}	$M_\infty^2 C_{L_{\text{upper}}}$	M_{lower}	$M_\infty^2 C_{L_{\text{lower}}}$	$M_\infty^2 C_{L_{\text{total}}}$
0.5	∞	1.43	0	0.27	1.70
0.5	1.55	1.00	0	0.27	1.27
0.5	1.5	0.97	0	0.27	1.24
1.0	∞	1.43	0	1.28	2.71
1.0	1.86	1.00	0	1.28	2.28
1.0	1.5	0.69	0	1.28	1.97
2.0	∞	1.43	0	9.75	11.18
2.0	4.97	1.00	0	9.75	10.75

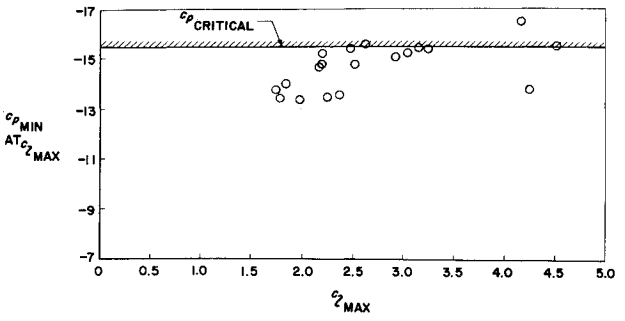

Fig. 13 Experimentally measured leading-edge minimum pressure coefficient at $c_{\ell_{max}}$ for a variety of two-dimensional high-lift configurations. Test Mach number = 0.20.

shown in Fig. 13, which is taken from Ref. 19. In tests of a considerable variety of two-dimensional models, it was observed that the lowest C_p on the model, at $c_{\ell_{max}}$ was nearly a constant equal to C_p^*. There is considerable scatter in the data of Fig. 13 because the tests were not planned to investigate C_p at $C_{\ell_{max}}$, but there is considerable evidence of a critical condition. If compressible C_p values can be calculated for an airfoil, an easy way of estimating $c_{\ell_{max}}$ is suggested by the figure—just find the c_ℓ at which C_p becomes sonic. All the tests were on airfoil sections where rear separation was not critical.

4. The Load-Carrying Capacity of Natural Boundary Layers

4.1 Introduction

This and the next section constitute the body of the paper. In combination, they expound the basic aerodynamics of mechanical high-lift systems. Until the 1960's, our analytical capability was insufficient to make quantitative calculations. Now, since the tools are here, it is time to put the whole story together, as best we know it. That is not to say that nearly all problems have been solved, but to a certain extent the remaining problems amount to just irritating details.

We go into considerable detail, and often rather elementary exposition, in the interests of making this part of the paper complete. The approach is motivated by the many misconceptions the author has encountered. For instance, with respect to slotted flaps, it has been suggested that if one just knew how to shape the airfoil, higher lift could be obtained with a one-piece airfoil, because the leakage from bottom to top allowed by the slots amounts to a kind of short circuit. Properly designed multielement airfoils are better, as will be shown. Another common statement is that a slot provides a kind of blowing boundary-layer control by the jet of "fresh" air that flows through it. How can it do that? It has no more total head than the ambient stream. Admittedly, that jet of "fresh" air has more energy than the boundary layer, but it only has freestream total head. At best, it may be a question of semantics. Later we shall see that the principal effect of a slot or slat is to reduce negative pressures, rather than to blow.

Sections 4 and 5 are a revision and, we hope, an improvement of Ref. 20, a paper given at an AGARD meeting. There are many papers and reports on the subject of high-lift devices, but their emphasis usually tends to be "how to." Ours is "why." One useful document is Ref. 21, which contains a large collection of lectures on the subject of high-lift devices. Another is Thain's,[22] which is an extensive review of the experimentally observed effects of Reynolds number on high lift. It too is more concerned with overall results than with explanation of the fundamental flow processes. Let it be noted that our discussion in these sections is confined to two-dimensional flow.

In view of Bernoulli's law, if a surface is to lift, the velocity over the upper surface must be speeded up. But we know that for any trailing edge, even the cusped type, the flow decelerates to below freestream values. Hence, to get more lift, we need higher velocities over the airfoil, but that in turn means greater deceleration towards the rear. The process of deceleration is critical, for if it is too severe, separation develops. The science of developing high lift, therefore, has two components: 1) analysis of the boundary layer, prediction of separation, and determination of the kinds of flows that are most favorable with respect to separation; and 2) analysis of the inviscid flow about a given shape with the purpose of finding shapes that put the least stress on the boundary layer. The two parts amount to a kind of applied-load and allowable-load problem. An analysis cannot be valid unless its elements are sound, so let us first look at the problem of predicting the onset of separation.

4.2 Accuracy of Predicting Separation Points

Because this question is so vital to many aerodynamic design problems, the accuracy of four leading methods was studied recently in Ref. 23, for the case of turbulent flows, which is the one of interest. The flows considered involved simple rear separation. Laminar bubble or laminar leading-edge separations were not considered. The main reasons are that proper design can eliminate them and that at high Reynolds numbers transition has occurred by the time adverse gradients appear. Fortunately, the problem we consider here is technically the more important, because the problem of separation after a laminar bubble and reattachment cannot be analyzed nearly as well. That is a problem for the future. There is no difficulty with simple laminar separation. It can be calculated to three- or four-place accuracy if the pressure input data have sufficient accuracy.

Four leading methods were examined: those of 1) Goldschmied, 2) Stratford, 3) Head, and 4) Cebeci-Smith. One case representative of the fairly large number examined in Ref. 23 is shown in Fig. 14. The separation point was carefully measured. The predicted separation points are marked on the pressure-distribution curves, which were supplied by the experiments. Goldschmied's method was erratic. The other three were in reasonable agreement, both in what is shown here and in the complete study,[23] Stratford's method tended to predict separation slightly early. The Cebeci-Smith method appeared best, with the Head method a strong second.

Hence, the Cebeci-Smith method has been chosen as the basic method, although much use is made of Stratford's

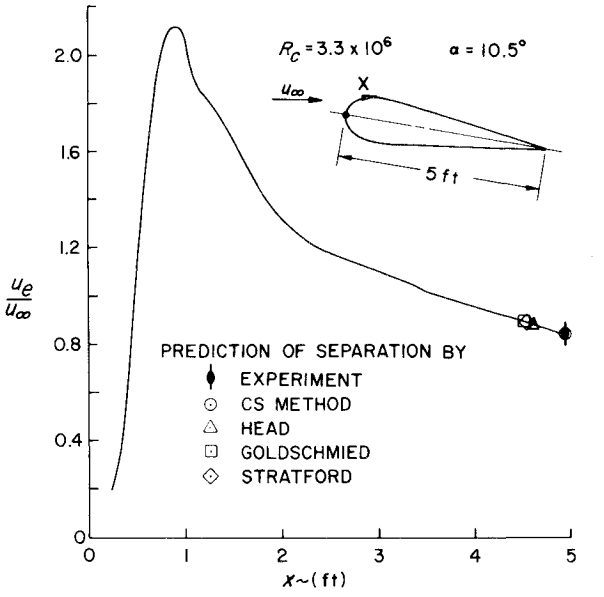

Fig. 14 Comparison with experiment of predicted separation points for Newman's airfoil.

method and ideas in this paper, mainly because of their great convenience. Figure 15 summarizes the prediction accuracy of the Cebeci-Smith method. The data consist of the results from Ref. 23 together with other, unpublished studies. One should not conclude from Fig. 15 that the general accuracy of turbulent-boundary-layer calculation is as good as it appears to be. Near separation, the accuracy of many of the boundary-layer quantities, such as the momentum thickness θ and the velocity profile, become poor. Nevertheless, accuracy of predicting the location of separation remains good. The Cebeci-Smith method predicts separation to be at the point where c_f, the local skin-friction coefficient equals zero.

In view of those results, the method of predicting separation appears to be accurate enough, in an engineering sense, to be used in determining relations, limits, and the like. It should be noted that the Cebeci-Smith method can handle with great accuracy the effects of Reynolds number or Mach number up to 5 or more. Also, it is the only one of the four methods that can analyze the case of axisymmetric boundary-layer flow.

4.3 Canonical Pressure Distributions

In almost all design work, pressure distributions are presented in terms of $C_p = (p - p_\infty)/(1/2\rho u_\infty^2)$. In that kind of presentation, high negative values of C_p invariably look bad, and one is unable to tell by inspection much about the margin of safety of the boundary layer against separation. Yet we know from basic scaling considerations that if two pressure distributions can be made congruent by proper scaling in the x- and C_p-directions, then the two flows are identical except for the Reynolds number effect, which is weak. Then, if separation occurs, it will be at the same scaled point for both flows. A particular 2-in. airfoil model at 100 mph will have very high values of velocity gradients, but a similar 200-in. model at 1 mph will have extremely low values. Yet the flows are exactly similar because their Reynolds numbers are the same. It is the dimensionless shape that counts. Hence it is particularly useful to scale out the magnitude of the velocity and also to scale out the chord. Where separation is important, the best scaling factor is the velocity just before deceleration begins. Because all pressure distributions are put in a standard form, it is natural to call them canonical pressure distributions and use a new variable $\bar{C}_p$. A typical one is illustrated in Fig. 16, which shows the idea and basic relations. The exact details of the normalization may well depend on the problem and the nature of the pressure distribution. The canonical pressure distribution, together with a Reynolds number, completely describes the flow. A meaningful Reynolds number is R_θ at the beginning of pressure rise. The left-hand part in Fig. 16 might represent the nose of an airfoil. Distance x is measured along the surface, but the origin of x is a matter of convenience. Often it is convenient to locate it at the beginning of pressure rise, as in the figure. Separation may occur at some point as noted. Because of the very simple relation between pressure coefficient and velocity ratio, the term pressure distribution is used indiscriminately for plots of either pressure coefficient or velocity ratio, provided that the flow is at low speed.

In the canonical system $\bar{C}_p = 0$ represents the start of pressure rise and $C_p = +1$ the maximum possible, that is, $u_e = 0$. Normally there are no negative values of $\bar{C}_p$. Furthermore, if two pressure distributions can be made congruent by proper scaling, a flow having a deceleration of $(u_e/u_\infty)^2$ from 20 to 10 is no more and no less likely to eparate than one decelerating from 1.5 to 0.75 or even from 0.10 to 0.05. The canonical plot is the one that is meaningful in separation analysis. With magnitude effects scaled out, much more can be told by a simple inspection than by a conventional plot. We dwell on the canonical pressure distribution at some length, because most working aerodynamicists do not realize its value. Figures 17 and 18 show conventional and canonical pressure plots for a typical high-lift airfoil. The basic charac-

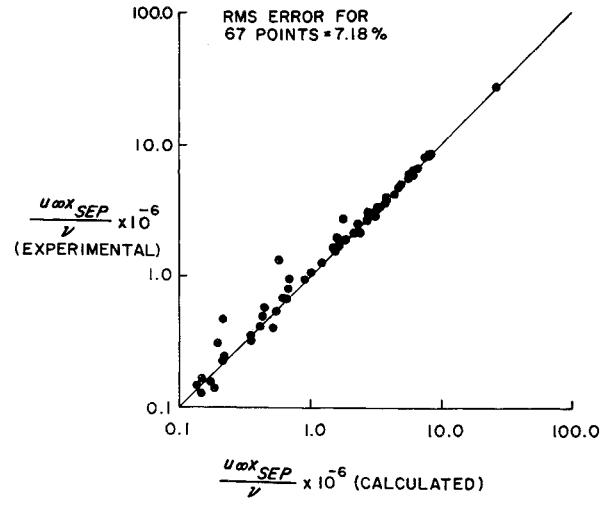

Fig. 15 Accuracy of predicting turbulent separation points by the Cebeci-Smith method.

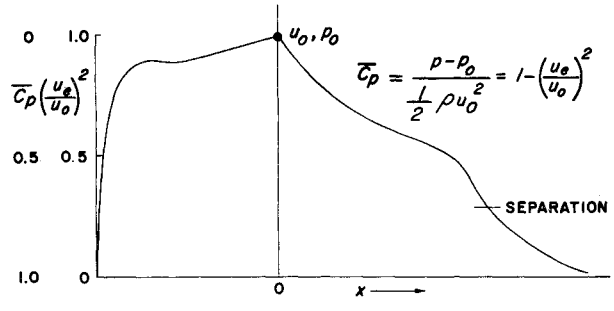

Fig. 16 A canonical pressure distribution, $\bar{C}_p(x)$.

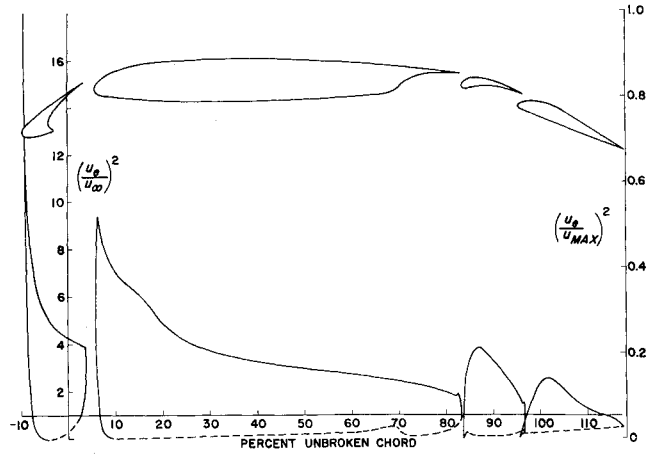

Fig. 17 A conventional theoretical C_p plot of a four-element airfoil. The right-hand scale is the canonical form, referred to peak velocity at the nose of the flap. $\alpha = 15°$, $\delta_f = 25°$, $\delta_s = 25°$, $c_\ell = 4.08$.

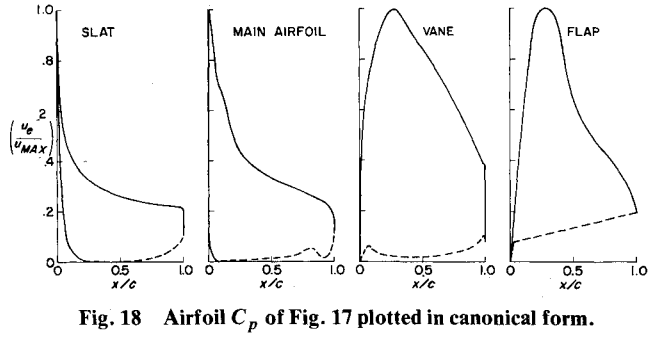

Fig. 18 Airfoil C_p of Fig. 17 plotted in canonical form.

ter of the four pressure distributions is much more apparent in Fig. 18. Figure 17 includes a canonical scale at the right, for the complete ensemble.

4.4 Relation between the Canonical Pressure Distribution and the Conventional

The relations between canonical and conventional pressure distributions are very simple, but because there has been confusion on the subject, they will be discussed at some length here. The canonical pressure distribution is easily related to the conventional form, where the reference velocity and pressure are u_∞ and p_∞. Because the square of the velocity is never negative, it is simpler to deal with velocity than with pressure coefficient. The fundamental relation is quite simple. It is

$$(u_e/u_\infty)^2(x) = (u_e/u_0)^2(x) \cdot (u_0/u_\infty)^2 \tag{4.1}$$

The last factor is just a constant. In many design problems, it is desirable to start with a canonical pressure distribution, then (u_0/u_∞) is not necessarily known and must be found. Construction of a canonical pressure distribution from a conventional one by means of Eq. (4.1) is trivial, because u_0/u_∞ is known. The method of converting velocities into C_p or $\bar{C}_p$ form is obvious from the given relations.

A problem of some importance is that of applying a canonical pressure distribution to the design of an airfoil by inverse methods. Somewhere along the pressure distribution the flow may separate. Then in the adaptation to the airfoil, the separation point should not be forward of the trailing edge. From Eq. (4.1) we can get the following equation:

$$\left[\frac{u_e}{u_\infty}\right]^2_{\text{sep}} = \left[\frac{u_e}{u_0}\right]^2_{\text{sep}} \left[\frac{u_0}{u_\infty}\right]^2 \tag{4.2}$$

Solving for $(u_0/u_\infty)^2$ substituting into Eq.(4.1), we get

$$\left[\frac{u_e}{u_\infty}\right]^2(x) = \frac{(u_e/u_\infty)^2_{\text{sep}}}{(u_e/u_0)^2_{\text{sep}}} \left[\frac{u_e}{u_0}\right]^2(x) \tag{4.3}$$

From general airfoil theory, we know that $(u_e/u_\infty)^2$ at the trailing edge is about 0.8, corresponding to $C_p = 0.2$. Then, for instance, if the canonical pressure distribution separates at $(u_e/u_0)^2 = 0.4$, the factor is $0.8 \div 0.4 = 2.0$. Of course Eq. (4.3) is valid, no matter where separation occurs, but an airfoil is not likely to be deliberately designed to have separation. If we assume separation is always to be at the trailing edge for any airfoil designed for maximum lift, we can specialize Eq. (4.3) to the form

$$\left[\frac{u_e}{u_\infty}\right]^2(x) = \left[\frac{(u_e/u_\infty)^2_{\text{T.E.}}}{(u_e/u_0)^2_{\text{sep}}}\right] \left[\frac{u_e}{u_0}\right]^2(x) \tag{4.4}$$

Observe that if by some artifice we could greatly increase $(u_e/u_\infty)^2_{\text{T.E.}}$, we could greatly increase $(u_e/u_\infty)^2(x)$ and hence the lift, all for the very same canonical pressure distribution. More will be said about that later. Equation (4.4) is easily converted to C_p form. Writing

$$C_p = 1 - (u_e/u_\infty)^2, \quad C_{p_{\text{T.E.}}} = 1 - (u_e/u_\infty)^2_{\text{T.E.}}$$

and

$$\bar{C}_p = 1 - (u_e/u_0)^2 \tag{4.5}$$

we have

$$C_p(x) = 1 - \frac{1 - C_{p_{\text{T.E.}}}}{1 - \bar{C}_{p_{\text{sep}}}} [1 - \bar{C}_p(x)] \tag{4.6}$$

4.5 Location of Separation in Two Families of Canonical Distributions

To exhibit the limits on the ability of a boundary layer to flow into regions of higher pressure, we present two plots, covering families of flows at two different Reynolds numbers, Figs. 19 and 20. The flows consist of a length of constant-velocity flow followed by a pressure rise described by the equation

$$\bar{C}_p = x^m \tag{4.7}$$

The unit Reynolds number is 10^6 per ft in Fig. 19 and 10^7 per ft in Fig. 20. Pressure rise is set to start at $x = 0$, but forward of that point are various lengths of flat-plate flow. It seemed more convenient to construct the plots in terms of feet and u_∞/ν rather than in terms of Reynolds number, although conversion into Reynolds number is easy. The total region of pressure rise is seen to be 1 ft. Four lengths of flat-plate run were studied: 1/64 ft, 1/16 ft, 1/4 ft, and 1 ft. The initial flows then developed boundary layers of various thickness at the beginning of pressure rise, as indicated by values of R_θ in the figures. The flat-plate flow is assumed to be entirely turbulent. If it were mixed laminar and turbulent, values of R_θ at $x = 0$ would be less and different.

Calculations of the flat-plate and $\bar{C}_p = x^m$ parts of the flow were then made by the Cebeci-Smith method until separation was reached. Lines cutting across the $\bar{C}_p = x^m$ curves mark separation points for the four lengths of flat-plate runs. The straight-line or concave pressure rises permit the greatest recovery before separation occurs. Also, the curves show that the amount of recovery is sensitive to the length of flat-plate run before the beginning of recovery. The separation loci, while indeed functions of the length of flat-plate run, are

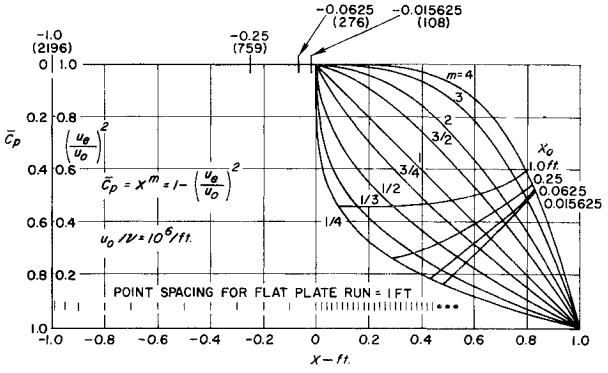

Fig. 19 Separation loci for a family of canonical pressure distributions. Point spacing used in the boundary-layer calculations for the 1-ft rooftop run is noted. Values in parentheses under origins of flow are values of R_θ at $x = 0$.

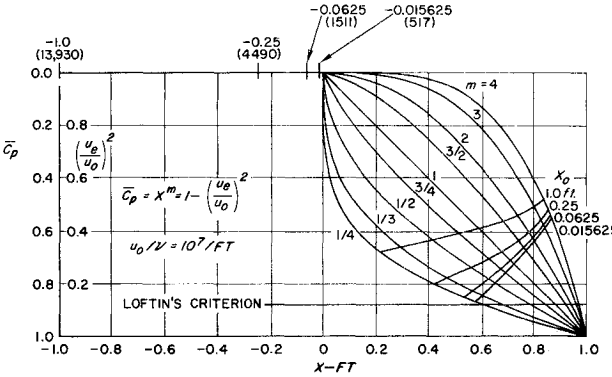

Fig. 20 Separation loci for a family of canonical pressure distributions. Loftin's criterion $\bar{C}_p = 0.88$ is noted.

more fundamentally functions of the boundary-layer thickness at the beginning of pressure rise. Hence, the separation loci could just as well be identified by the noted values of R_θ at the beginning of pressure rise. Then Figs. 19 and 20 become applicable for any combination of rising pressure and transition. For any arbitrary forward flow, one would then calculate R_θ at $x=0$ and interpolate between the loci as a function of R_θ. In brief, we are saying that any flow that develops one of the set of values of R_θ and that has the same aft flow will have the same separation point as that of a forward flow developed by an equivalent run of flat plate. The equivalence is not rigorous, because a separation point is a function not only of initial R_θ but also of the shape of the profile as described by H. But R_θ is the dominant parameter, and, considering the accuracy of turbulent boundary-layer calculations, it is the only one that need be considered here. With u_0/ν specified θ converts to R_θ as the interpolation parameter.

These comments point out the fact that extensive laminar flow in the forward part helps to delay separation considerably, because it reduces R_θ. Furthermore, boundary-layer suction forward of the pressure rise would delay separation. Another fact that is surprising is that if the pressure rise is not too great, it may be extremely steep; in fact, $d\bar{C}_p/dx$ may be nearly infinite. (Owing to the use of finite steps, the slope of $\bar{C}_p$ is never quite infinite in the Cebeci-Smith method. If it were, a constant in the partial differential equation would be infinite and the method would fail.) In the next section, we see that the infinite rate of pressure rise is confirmed by Stratford's equations, which he derived by an analytic approach.

Loftin and von Doenhoff[24] studied a large number of thin airfoils and arrived at a separation criterion that in our terms is $\bar{C}_p=0.88$. It is plotted in Fig. 20. A thin airfoil at angle of attack has an effective forward flow about the same as that of the $x=1/64$-ft distance, and the pressure-rise region is approximated by the $m=1/3$ or $m=1/4$ curve. Hence, we see that Loftin's criterion is rather closely predicted by the charts. But we also see that it is far from universal.

The set of charts provides an "eyeball" method for estimating separation points. We shall illustrate by considering Fig. 14. Try to relate that flow to one of the canonical plots. If the pressure distribution of Fig. 14 is replotted in u_e^2/u_∞^2, or canonical form, the rear flow looks approximately like the $x^{1/3}$ flow and the front flow is effectively quite short. Transition was measured at $x=1.169$ ft. Hence the logical equivalent flat-plate length is 0.015625 ft. Which chart should be used? Probably Fig. 20. To use the figures, convert the chord of the airfoil to 1 ft. Because it is so small, there is no need to be concerned about the 0.015625 forward part. In order to hold Reynolds number at 3.3×10^6 with the reduced chord, we need to increase u_∞/ν to 3.3×10^6/ft. But the charts are in terms of u_0/ν. Now from Fig. 14, $u_0/u_\infty=2.1$. Hence, $u_\infty/\nu=3.3\times10^6$ corresponds to $u_0/\nu=7\times10^6$. Then Fig. 20 seems to be the better of the two to use. Of course, interpolation between the two is possible. From Fig. 20 for $m=1/3$, we find that separation occurs at $(u_e/u_0)^2=0.17$ or $u_e/u_0=0.41$. In Fig. 14 $(u_e/u_\infty)_{\max}=2.1$. Hence separation should occur at about $0.41\times2.1=0.87$, a ratio that is satisfactorily close to the measured separation point. More care in the analysis probably would increase the accuracy. For instance, a careful calculation of R_θ at $x=0$ by Truckenbrodt's method would be better than a guess. Also, the exponent in the pressure-rise region could be determined more accurately by the use of log graph paper.

The canonical plots contain much useful information. For instance, if load is being carried by an airfoil in cruise, the pressure rise at the trailing edge is not great. If it corresponds to $\bar{C}_p=0.4$, any m-curve will sustain the pressure rise, and therefore suitable airfoils with all kinds of pressure distributions can be made. But if one is striving for all the lift he can get, the pressure-rise curve for $m=1/4$ or $1/3$ is the best, because that gives the greatest ratio and the highest mean value of $\bar{C}_p$ along the upper surface.

Reference 20 gives two charts for a different family of pressure distributions; they are arcs of circles. Results are not significantly different from those of the $\bar{C}_p=x^m$ family. Furtheremore, Ref. 20 contains an additional pair of charts for the case where $\bar{C}_p=x^m$ at $M_o=1$. The separation loci are considerably different, but more of the difference appears to be eliminated if we consider the flow

$$1-(u_e/u_0)^2=x^m \tag{4.8}$$

The expression for $\bar{C}_p$ when the flow is compressible is

$$\bar{C}_p=\frac{2}{\gamma M_o^2}\left\{\left[1+\frac{\gamma-1}{2}M_o^2\left(1-\frac{u_e^2}{u_o^2}\right)\right]^{\gamma/(\gamma-1)}-1\right\} \tag{4.9}$$

If $u_e/u_0=0$, $\bar{C}_p=1.28$ at $M_o=1$; and if $\bar{C}_p=1.0$, $(u_e/u_0)^2=0.18$. Hence, at $\bar{C}_p=1.0$, the flow is still far from stagnation. Therefore, the better canonical compressible flow to consider is the flow in terms of $(u_e/u_0)^2$. Some points calculated thus for flow at $M_o=1.0$ are shown in Fig. 8 of Ref. 20. The answer to the question of whether compressibility aggravates separation depends on the reference. Certainly, compressibility aggravates pressure gradients on a given body, which implies earlier separation. When considered in $\bar{C}_p$ form, compressibility is favorable. Hence the most fundamental approach appears to be to consider the problem in terms of u_e/u_o^2, which is a measure of the kinetic energy of the flow that remains. In that form, at least to $M_o=1.0$, the effects of compressibility are minor when considered from the basic canonical standpoint.

In closing this section, we remark that because of the analytic nature of our canonical pressure distributions $\bar{C}_p=x^m$, it is very easy to apply Stratford's criterion. That has been done. If Stratford's predictions had been added to the plots of Figs. 19 and 20, the differences in separation loci would appear considerable. Still they are so small that use of the charts and the findings is not negated. Addition of Stratford-type loci would only cause confusion. Therefore, we show only one type of calculation, the Cebeci-Smith, which in general is believed to be the most accurate. Furthermore, it should be noted that Figs. 19 and 20 differ from their earlier forms in Ref. 20. The main reason is that here we used the analytic nature of the $\bar{C}_p=x^m$ flows to compute certain necessary derivatives.. In the earlier work, finite-difference formulas were used. Disagreements such as those just indicate the state of the art of turbulent-flow calculation.

4.6 Limiting Canonical Distributions

The $\bar{C}_p=x^m$ families are very useful for almost all practical flow problems, but of course the shapes of the $\bar{C}_p(x)$ curves are arbitrary; the shapes are selected as a matter of analytical convenience. Just as in many other problems, there is one shape that is "best," Stratford's solution. We do not mean to imply that the solution is exact, but as is indicated by Fig. 14, it has acceptable accuracy. Stratford has derived a formula, Ref. 25, for predicting the point of separation in an arbitrary decelerating flow:

$$\frac{\bar{C}_p[x(d\bar{C}_p/dx)]^{1/2}}{(10^{-6}R)^{1/10}}=S \tag{4.10}$$

where if $d^2p/dx^2\geq0$, then $S=0.39$; or if $d^2p/dx^2\leq0$, then $S=0.35$. Also, $\bar{C}_p\leq4/7$. The flows examined consist first of a flat-plate flow, just as with $\bar{C}_p=x^m$ flows. Hence, x is distance measured from the leading edge of the plate, and $R=u_ox/\nu$. If the flows begin the pressure rise at a point x_o such that $\bar{C}_p=(x-x_o)^m$, left-hand side of Eq. (4.10) starts from a zero value, provided that $m>1/3$. The left-hand

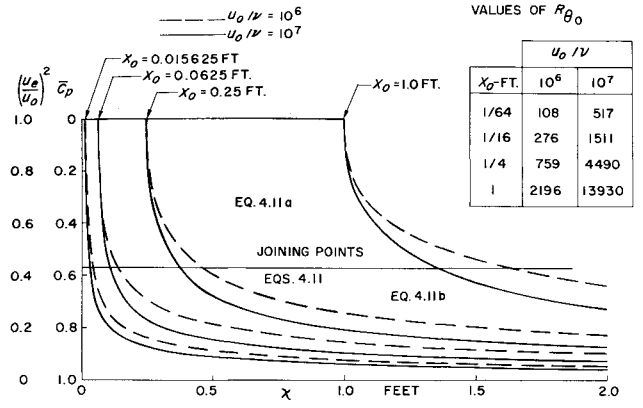

VALUES OF R_{θ_0}

x_o-FT.	u_o/ν 10^6	10^7
1/64	108	517
1/16	276	1511
1/4	759	4490
1	2196	13930

Fig. 21 Stratford limiting flows at two values of unit Reynolds number.

side then grows. When it reaches the limiting value of S, separation is said to occur. The study of Ref. 23 showed the constants to be slightly different, but here, for our purposes, we accept Stratford's values. See Ref. 25 for further details.

If S is held at its limiting value of 0.39 for $d^2p/dx^2 \geq 0$, Eq. (4.10) amounts to an ordinary differential equation for $\bar{C}_p(x)$. It is evident from Eq. (4.10) that the equation describes a flow that is ready everywhere to separate. Stratford presents the following solutions:

$$\bar{C}_p = 0.645\left\{0.435\, R_o^{1/5}[(x/x_o)^{1/5} - 1]\right\}^{2/n}$$

$$\text{for } \bar{C}_p \leq (n-2)/(n+1) \tag{4.11a}$$

and

$$\bar{C}_p = 1 - \frac{a}{[(x/x_o)+b]^{1/2}} \quad \text{for } \bar{C}_p \geq \frac{n-2}{n+1} \tag{4.11b}$$

In that two-part solution, x_o is the start of pressure rise, $R_o = u_o x_o/\nu$, x is the distance measured from the very start of the flow, which begins as flat-plate, turbulent flow. The number n is a constant that Stratford finds to be about 6. The quantities a and b are arbitrary constants used in matching values and slopes in the two equations at the joining point, $\bar{C}_p = (n-2)/(n+1)$. Of course, Eq. (4.11a) describes the beginning of the flow, and Eq. (4.11b) the final part. The flow is an equilibrium flow that always has the same margin, if any, against separation.

Two families of such flows have been computed; they are shown in Fig. 21. They correspond to the same set of conditions that were used in the $\bar{C}_p = x^m$ flows. As has already been mentioned, they represent true limiting flows—the slightest increase in adverse gradient anywhere should cause separation. The curves assume the length of flat-plate runs indicated, but just as for the $\bar{C}_p = x^m$ families, what is of more fundamental significance is the boundary-layer thickness at the beginning of pressure rise. Hence, a table of initial values of R_θ is included. With the aid of those R_θ values, the curves could be applied to arbitrary forward pressure distributions having mixed laminar/turbulent flow.

Within the accuracy of the theory, which tests have proved to be correct and somewhat conservative, those curves show the fastest possible pressure rise that can be obtained from a natural boundary layer. Also, when compared with Cebeci-Smith predictions, the theory appears conservative. Figure 21, together with Eq. (4.11), exhibits the following features:

1) The initial slope $d\bar{C}_p/dx$ is infinite, so that small pressure rises can be made in distances from very short to zero.

2) It is easy to show that $\bar{C}_p \sim x^{1/3}$ in the early stages.

3) The dominant variable is x/x_o [see Eq. (4.11)]. Hence, when x_o is small (i.e., the boundary layer is thin), pressure recoveries may be very rapid. When the initial run is long and the boundary layer is thick, the allowable average pressure gradient is much less. Or conversely, thick boundary layers are much more likely to separate than thin.

4) The unit Reynolds number effect is rather small [see Fig. 21 and Eq. (4.11a)].

5) Theoretically, 100% of the dynamic pressure can be recovered, but the distance required is infinite.

6) Aside from error in the theory, the curves of Fig. 21 are the shortest possible pressure recoveries—they are the "end of the line." Nothing better can be done except by boundary-layer control.

7) The Stratford pressure distribution is the path of least resistance connecting two pressure points A and B, as will now be shown.

If we accept quadrature formulas such as Spence's or Truckenbrodt's, then Stratford's flow is found to be the minimum-drag flow. Consider the flow situation sketched in Fig. 22. We wish to go from some point A to another point B. Various paths may be possible, as sketched. The Stratford path is the path of lowest drag. We shall show this by means of Truckenbrodt's formula.[26] For purposes of demonstration, we can write it as follows:

$$\theta_B = \left[\theta_A + K\int_{x_A}^{x_B} \left(\frac{u_e}{u_\infty}\right)^{3.33} dx\right]^{6/7} \tag{4.12}$$

The path that developes the minimum value of the momentum defect θ_B at B will be the path of minimum drag. It is obvious by inspection that the Stratford path is the answer. For it, the Truckenbrodt-type integral is minimum. As has already been shown, any curve below Stratford's would suffer from separation. According to this method of analysis, the best path is Stratford's, even if it means a sudden jump upward in velocity as sketched at B. Exactly how this flow can be applied to airfoil design is uncertain, in general, because of all the interacting effects. But at least we should be able to say that when a Stratford flow is applied in a sound fashion, low drag can be expected.

The first part of Eq. (4.11a) of the pressure rise is quite rapid, but the final part, Eq. (4.11b), is quite slow. It is enlightening to compare with a lossless two-dimensional diffusor as sketched in Fig. 23, which provides a simple physical picture. In canonical form, (with, V as velocity) the pressure coefficient referred to conditions at $x = 0$ is

$$\bar{C}_p = 1 - (V^2/V_o^2) \tag{4.13}$$

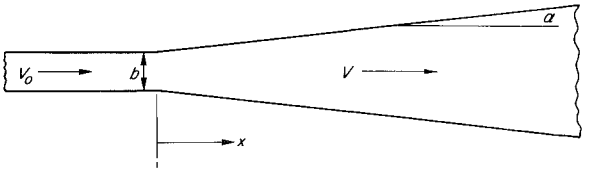

Fig. 22 Possible pressure distributions connecting points A and B.

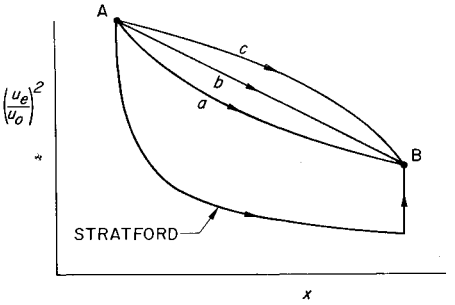

Fig. 23 Two-dimensional diffuser.

The width of the diffuser is $w=b+2x \tan \alpha$. When that expression is combined with the equation of continuity and substituted into Eq. (4.13), we have

$$\bar{C}_p = 1 - \frac{1}{[1+(2x/b)\tan\alpha]^2} \tag{4.14}$$

a formula whose structure is generally like that of Eq. (4.11b) in the sense that an infinite distance for full recovery is indicated. But the exponent of the denominator is 2 for the diffuser, as compared to 1/2 for Stratford's flow.

A Stratford flow has a continuous margin of safety over its entire length with respect to separation, whether at the beginning of pressure rise or far, far downstream. The margin of safety can be adjusted by changing the constant S in Eq. (4.10).

Both Eqs. (4.11b) and (4.14) show that an infinite distance is required to bring a flow in the boundary layer to complete rest. Now if a round-nosed object is placed in a stream, it generates a stagnation point. Then, if a round-nosed object like a cylinder is placed on end on the floor of a wind tunnel, the situation is such that a boundary layer is brought to rest in a finite distance, with separation sure to occur. (It is believed that the three-dimensionality of the flow does not negate that conclusion.) Airplanes often have similar intersections—wing-fuselage, for example. The inevitability of separation in such cases does not seem to be fully appreciated. The inevitable separation is one of the justifications for filleting.

4.7 Limiting Suction Lift

By means of the relations in Sec. 4.4, the Stratford canonical distributions of Fig. 21 can be transformed into idealized airfoil-upper-surface pressure distributions. A key parameter in the conversion is the effective velocity at the trailing edge, that is, the effective edge velocity to which the forward flow must decelerate when a boundary layer exists. Without the boundary layer, airfoils that ended with a finite trailing-edge angle would always have zero final velocity. The effective velocity we are talking about is really a correlating velocity. Edge velocities at the 97- or 98-% chord point are good values. Because the flow over an airfoil may be accelerated, retarded, heated, sucked, blown, reenergized, and finally discharged "overboard," the author tends to think of the boundary-layer air as going through a sort of physical process and then being "dumped" overboard. Hence, he likes to refer to the effective leaving velocity by a homely name—dumping velocity.

Observation of various pressure distributions shows that a typical effective trailing-edge velocity or "dumping velocity" is $(u_e/u_\infty)^2=0.8$. If we use this value, we can form two main families of limiting upper-surface pressure distributions, one for full laminar flow along the rooftop and one for full turbulent flow. Some results are presented in Figs. 24 and 25 for a chord Reynolds number of 5×10^6. Figure 25 amounts to a direct scaling of the standard Stratford flow, because the rooftop is assumed to be entirely turbulent. In Fig. 24, the rooftops are considerably longer, because with laminar flow a longer distance is required to develop the same value of R_θ as that developed by a run of fully turbulent flow.

All the flows of Figs. 24 and 25 have the property of producing the same final velocity without any separation but with the most rapid possible pressure rise from various rooftop C_p-levels. If the rooftop C_p is very high, the pressure rise must start early. If low, it can start late. If areas within the curves are calculated, it is found that a maximum exists and that the initial negative C_p for this condition is not very high. Values of the upper-surface lift coefficients are noted on the

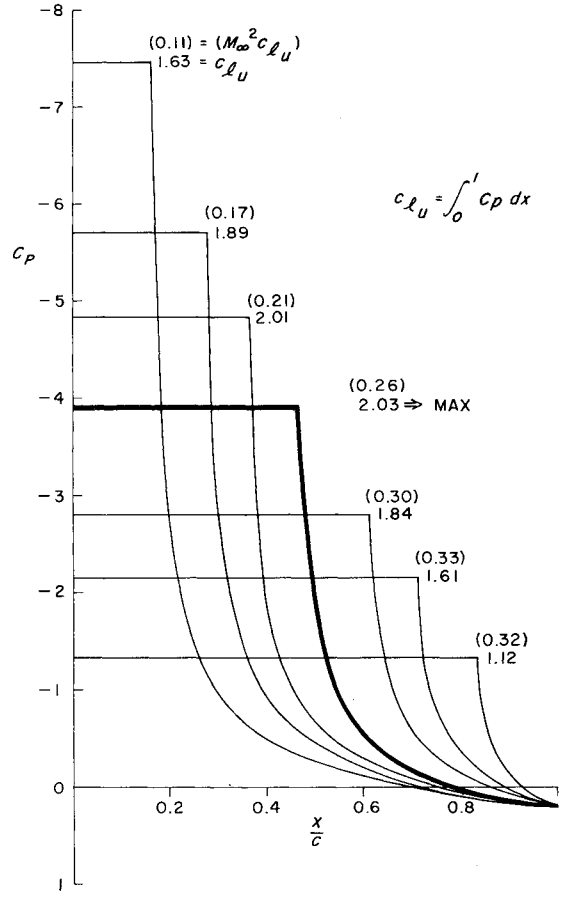

Fig. 24 Suction side pressure distributions using Stratford pressure recovery to $C_p=0.20$ at trailing-edge. Laminar rooftop, $R_c=5 \times 10^6$. Values beside each curve indicate the lift that is developed. In the $M^2{}_\infty c_l$ form M_∞ is that value which just makes the peak velocity sonic according to the von Kármán-Tsien formula.

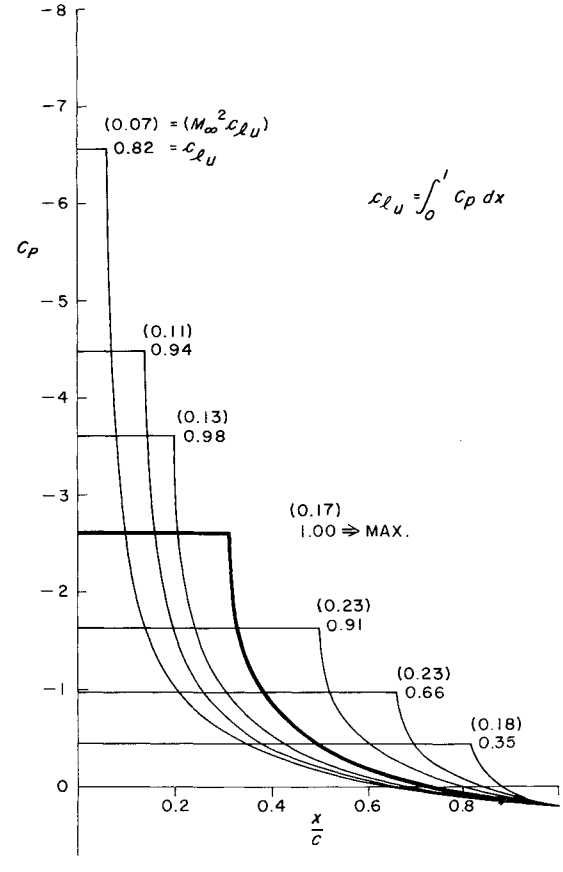

Fig. 25 Suction side pressure distributions using Stratford pressure recovery to $C_p=0.20$ at trailing edge. Turbulent rooftop. $R_c=5 \times 10^6$.

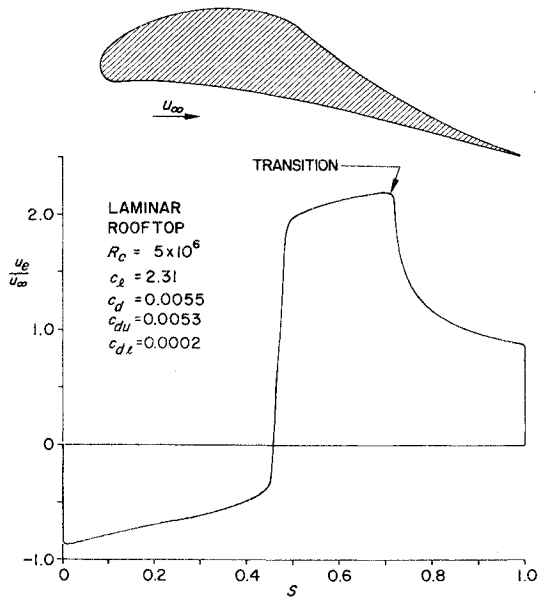

Fig. 26 An optimized high-lift Liebeck airfoil that uses a Stratford pressure recovery. Values noted are theoretical. S is peripheral distance measured from the trailing edge. Pat. Pend.

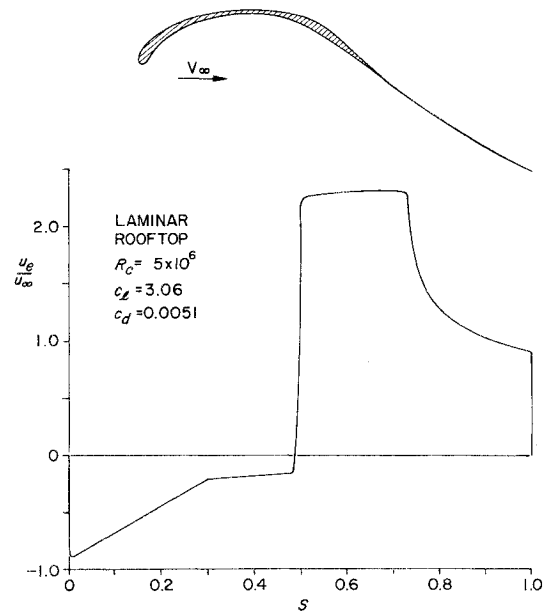

Fig. 27 The Liebeck airfoil that produces maximum lift with fully attached flow, design $R_c = 5 \times 10^6$. Pat. Pend.

figures. For laminar and for turbulent approach flow, the maximum suction-surface lift coefficients are 2.03 and 1.00, respectively. Higher Reynolds numbers would increase these values. It is interesting to note the very strong theoretical effect of laminar flow on lift. Usually, we think that the main benefit of laminar flow is reduction of drag.

We have been discussing lift coefficient analysis. A second and perhaps more important subject is the maximum force or $M_\infty^2 c_\ell$ that we talked about in Sec. 3. The problem cannot now be solved as accurately as for incompressible flow by means of Stratford's analysis. A compressible Stratford-type solution is necessary as a minimum. Nevertheless, nothing prevents us from determining critical Mach numbers for each of the pressure distributions by Kármán and Tsien's rule and assuming that the pressure distributions are still valid. If so, we get the values of $M_\infty^2 c_\ell$ in parentheses in Figs. 24 and 25. Again there is a maximum value. For laminar flow it is 0.33. The maximum occurs at much lower lift coefficients.

In the two figures, the y-ordinate was scaled to produce $(u_e/u_\infty)^2 = 0.8$ at the trailing edge. Suppose that we could by some means raise the number to 1.2. Then by Eq. (4.4) all values would be increased 50% and a 50% gain in lift would result. Therefore, a high dumping velocity is very important.

4.8 Examples

Within the accuracy of the theory, we have just shown in an idealized form the maximum suction lift that can be developed with fully attached flow when the flow is that in a natural boundary layer. R. H. Liebeck[27] was greatly responsible for the basic studies. He has recently applied them to actual airfoil design, where lower-surface pressure, upper-surface pressure, and shape must all be considered. Furthermore, he formulated the problem exactly, working in terms of surface distance and circulation instead of pressures projected on a plane, as in Figs. 24 and 25. The formulation leads to an inverse airfoil design problem that can be solved with great accuracy by James' method[28] or other good inverse methods.

One such solution is given in Fig. 26. To be sure of developing laminar flow on the upper surface, the forward part was given a favorable gradient instead of just a constant velocity flow, as in Figs. 24 and 25. Theoretical values of c_ℓ and c_d are shown on the figure. The section L/D is 420. Tests, Ref. 27, of two airfoils of the type shown in Fig. 26 show almost perfect agreement between theory and experiment at

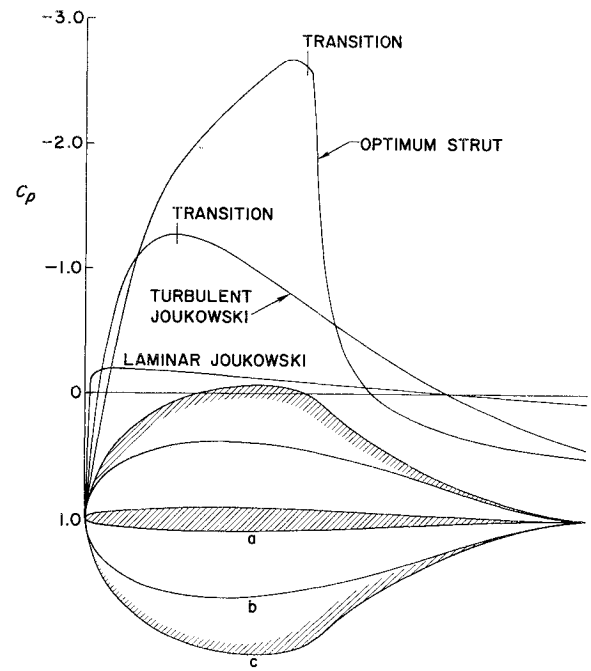

Fig. 28 The thickest struts having fully attached flow.

the design point. One of the most remarkable features of the airfoil is the extremely low theoretical drag of the lower surface. As can be seen from the pressure distribution, the velocity on the lower surface is not only low but is accelerating continuously from nose to trailing edge. Hence, it is likely to be laminar all the way. The upper-surface drag is relatively low too, partly because of the minimum-drag property of Stratford flows (Sec. 4.6, property 7).

Liebeck's work was begun in an attempt to answer the question, "What is the maximum lift that can be developed by a single-element airfoil with fully attached flow, and what is the shape required to develop it?". At $R_c = 5 \times 10^6$, for all practical purposes, Fig. 27 gives the answer. The airfoil has substantially zero thickness, because at design conditions

thickness is harmful, as a little thought will indicate. This limiting airfoil develops a section L/D of 600! Conventional airfoils rarely exceed 180.

Although they are not related to the high-lift problem, we shall close this section with some interesting examples of what can be accomplished by various kinds of boundary-layer flows. By showing some limiting shapes, Fig. 28 demonstrates the ability of various types of boundary-layer flows to withstand adverse pressure gradients. All three shapes are cusped in order to eliminate the rear stagnation point that theoretically accompanies a finite-angle trailing edge. All boundary-layer calculations were made for the naked shapes. A slight relief would be provided if the effects of boundary layer were taken into account. Hence, the bodies shown here have a slight degree of conservatism. The first cases represent the thickest symmetrical Joukowski strut that can have complete laminar flow without any laminar separation. It is only 4.6% thick. The Reynolds numbers must be low; otherwise the flow would become turbulent. The intermediate case is a Joukowski strut having mostly turbulent flow with transition as shown in the figure. The chord Reynolds number is 10^7. Finally, if we pull out all stops and so shape the forward gradients as to be favorable to laminar flow and then use the Stratford pressure recovery in the rear, we obtain the thickest shape, which is more than 53% thick. The theoretical Michel transition point is marked on the figure. With the strong favorable pressure gradients, there should be no trouble in obtaining the required laminar flow, even at the rather high Reynolds number of 10^7. Like the high-lift shapes, it too was designed by the James method. Because of the extensive laminar flow, the theoretical value of c_{d_p} is only 0.0077, in spite of the great thickness.

4.9 Off-the-Surface Pressure Recovery

Until now, our concern has been with fluid flowing into regions of higher pressure while it is in contact with a surface, that is, a decelerating boundary-layer flow. But there can be another kind of flow, the flow of wakes that may be out of contact with any wall, into regions of higher pressure. Such a flow occurs, to a degree, on any multielement airfoil. A slat develops its own boundary layer, which flows off its trailing edge, forming a wake of low-energy air that now flows alongside the rest of the airfoil and on downstream. Consider the geometry of Fig. 17, for instance, or the streamline pattern of Fig. 29. Each forward element produces wake components over its downstream partners.

The theory of that kind of wake flow is not nearly so well developed as the theory of boundary-layer flow. Therefore, we shall be content to given only a brief discussion of its features, chiefly for the purpose of calling attention to them. There can be two kinds of wakes flowing into a region of higher pressure. One is separated from the adjacent boundary layer by a region of potential flow. That kind occurs when gaps are large. The other kind is so close to the adjacent boundary layer that the two flows finally merge and become one thicker boundary layer. That kind occurs when gaps are small. By some it is called confluent boundary-layer flow.

Because a wake is usually near the main airfoil surface, the pressures impressed on it are little different from those on the airfoil surface; for example, consider the streamline in Fig. 29

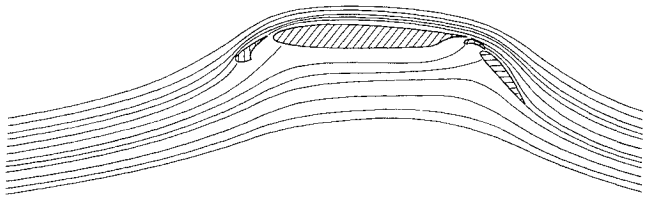

Fig. 29 Calculated streamline flow field for airfoil with leading edge slat and double slotted flap, $\alpha = 0°$, $c_\ell = 3.70$.

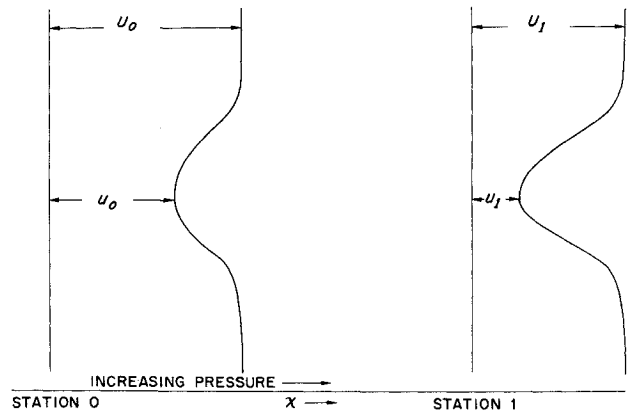

Fig. 30 Flow of a wake into a pressure rise.

that leaves the slat. If the pressure rise is great enough, we can have flow reversal in the stream, entirely off the surface. The phenomenon is easily demonstrated by resorting to Bernoulli's equation. Consider a flow as illustrated in Fig. 30. At station 0, there is a flow in which static pressure is constant across the stream, but there is a wake-like portion in which velocities are deficient. The wake flows into a region of higher pressure at station 1. What happens to the wake region? Because we are considering regions very thin with respect to any overall curvature of the flow, it is reasonable to assume that the static pressure p_1 at station 1 is also constant across the boundary layer. Because gradients $\partial u/\partial y$ will be small, the shear stresses will be low and then it is a good approximation to assume that each streamline maintains its total head between station 0 and station 1. Such an assumption has been confirmed in numerous analyses, including Stratford's. Hence, using U for potential regions and u for energy deficient regions, we can write, for incompressible flow,

$$p_o + \tfrac{1}{2}\rho U_o^2 = p_1 + \tfrac{1}{2}\rho U_1^2 \tag{4.15}$$

and

$$p_o + \tfrac{1}{2}\rho u_o^2 = p_1 + \tfrac{1}{2}\rho u_1^2 \tag{4.16}$$

Solve for U_1^2 and u_1^2 and obtain their ratio, thus:

$$\frac{u_1^2}{U_1^2} = \frac{p_o - p_1 + 1/2\rho u_o^2}{p_o - p_1 + 1/2\rho U_o^2} \tag{4.17}$$

Now introduce our canonical pressure coefficient $\bar{C}_p = (p - p_o)/(1/2)\rho U_o^2$ into (4.17). We obtain

$$\frac{u_1^2}{U_1^2} = \frac{(u_o^2/U_o^2) - \bar{C}_p}{1 - \bar{C}_p} \tag{4.18}$$

The equation shows that as $\bar{C}_p$ increases, u_1^2/U_1^2 can reach zero well before $\bar{C}_p$ reaches $+1$, provided that $u_o^2/U_o^2 < 1$. For example, if $u_o^2/U_o^2 = 1/2$, $u_1^2/U_1^2 = 0$ when $\bar{C}_p = 1/2$. That is, the velocity-defect ratio is magnified, and flow reversal can occur in the main stream. Viscosity, of course, helps to smooth out the wake velocity defect, which means that a Bernoulli approach is unduly conservative.

According to Eq. (4.18), if flow is into a region of higher pressure, the velocity defect ratio always worsens. Opposing it is the effect of viscosity, which tends to smooth out the defect. Gartshore[29] has derived an approximate test as to whether the wake grows or decays. It is

$$\frac{1}{1 - C_p}\frac{dC_p}{dx} = \frac{1}{1 - \bar{C}_p}\frac{d\bar{C}_p}{dx} > \frac{0.007}{\delta^*} \tag{4.19}$$

where δ^* is the displacement thickness of the wake at the point being considered. If the left-hand side of Eq. (4.19) is less than $0.007/\delta^*$, the wake decays; if greater, it grows.

To study the structure of Eq. (4.19), we shall apply the test to a flow that is a variation of the $\bar{C}_p = x^m$ flows shown in Fig. 20. Referring to that figure, we shall assume that we have flat-plate flows of various lenths, from 0.015625 to 1.0 ft, that develop boundary layer on both sides, All end at $x=0$. They then dump their boundary layers into the $\bar{C}_p = x^m$ pressure region. Will the wake defect amplify or decay? First we must know the initial displacement thickness of the wake. Assume it to be equal to the final displacement thickness of the boundary layer from both sides of the plate. A convenient formula is Blasius 1/7-power formula

$$\delta^*_{1\text{ side}} = \frac{0.0463\ell}{R_\ell^{1/5}} \tag{4.20}$$

After substitution from (4.20) into (4.19), we obtain

$$\frac{1}{1-\bar{C}_p}\frac{d\bar{C}_p}{dx} > \frac{0.075R_\ell^{1/5}}{\ell} \tag{4.21}$$

where ℓ is the length of the flat plate and $R_\ell = u_0\ell/\nu$. Figure 31 shows the results. The two sides of Eq. (4.21) are plotted separately. When the left-hand side exceeds the right-hand side, instability develops. The $m=1$ curve is a special dividing case. It begins with the value of 1.0. Any higher value of m begins with the value 0; any lower value of m, the value ∞. Hence, according to Gartshore's criterion, the wake is always initially unstable for $m<1.0$. The figure shows a strong effect of wake thickness upon the stability. For our problem a higher Reynolds number is favorable because it reduces δ^* and hence increases the value of the right-hand side of Eqs. (4.19) or (4.21), but the effect is weak. According to Eq. (4.21), for the $\bar{C}_p = x^m$ flows the left-hand side ultimately approches infinity, and therefore any of the wake flows should finally go unstable. Hence, with $m<1$, theoretically we have a situation where the wake flow is unstable to begin with, but quickly becomes stable and finally becomes unstable again if carried far enough. Whether that indeed is true is not known.

However, according to Gartshore's analysis, a boundary layer is more prone to separation than the wake is to instability. Consider the $\ell=0.25$-ft plate in Fig. 31. For any of the m-values, the final instability is at $x\simeq 0.8$ ft. However according to Fig. 20, for most values of m, the boundary-layer flow has separated earlier.

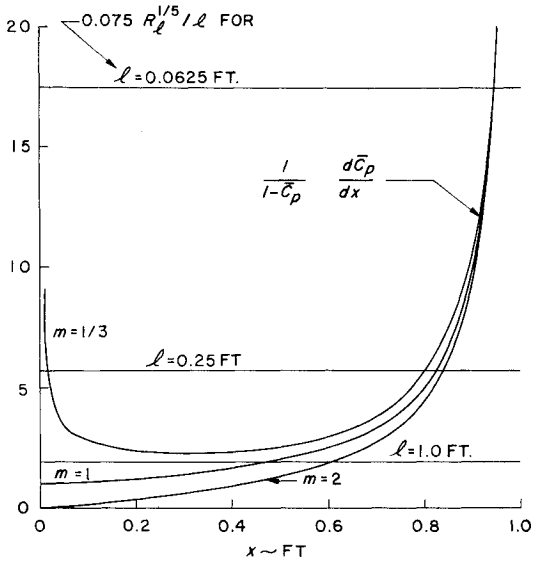

Fig. 31 Evaluation of Eq. (4.21) for the decelerating flows of Fig. 20, $u_0/\nu = 10^7$.

Gartshore cites experimental evidence that confirms his deductions. It was obtained by examining flow over deflected plain flaps. Without doubt, the effect can and has occurred—separation off the surface. But since there has been very little study of that kind of flow, the validity of relation (4.21) is in question. Especially in question are some of the derived consequences, such as the initial instability for some fractional values of m. For example, when $m = 1/3$ and $1/2$, a boundary-layer flow would not separate, but the wake flow would be unstable. The principal purpose in presenting example applications is to get the concept into the open, and at least exhibit in a qualitative way the effect and the interaction between wake thickness and pressure gradient.

In practical applications, with their lack of infinite adverse gradients through which a wake must flow, the wake-instability problem should rarely be critical, which means that wakes can endure pressure rises that boundary layers cannot endure. What a multielement airfoil does then, in effect, is to use two methods of pressure recovery: the conventional, that is, on-the-surface pressure recovery, and off-the-surface pressure recovery. On a slatted airfoil, for instance, the history of the flow is this: Air flows over the slat, reaches a peak velocity, then decelerates in contact with its surface, leaves the surface and continues to decelerate until trailing-edge pressures are reached, after which it gradually accelerates back to freestream conditions. By the off-the-surface deceleration, recovery from very high negative C_p values can be made in much shorter distance than can be made when all the deceleration is in contact with a surface.

On the right-hand side of Fig. 17 is a canonical pressure scale based on the maximum velocity on the slat. According to that scale, the final velocity-squared ratio at the trailing edge is only 0.025. If all the deceleration had been in contact with the surface, the flow would surely have separated, according to Figs. 19 and 20.

Nothing so far has been said about the case when boundary layers merge. Lockheed [30,31] has studied the problem and, in fact, has developed a general method for analyzing confluent boundary layers. But because of the complicated nature of the flow, bold simplifications had to be made. Like Gartshore's analysis, the methods need development and further checks by detailed experimental work. Improved methods for both the merging and the nonmerging wake flows are problems for future work.

It is our observation, as well as that of Foster et al. [32], that gaps between airfoil elements should be so large that wakes and boundary layers do not merge for, if they do, early separation will set in. In fact, Foster et al. in discussing the subject makes the following statement:

"...when the flap is in the optimum position from the viewpoint of obtaining the highest maximum lift, the interaction between the wing wake and the flap boundary layer is comparatively mild, with the two layers retaining their separate identity almost to the flap trailing edge."

Hence, we are somewhat fortunate. Optimum designs are outside the region of merging boundary layers, and, furthermore, flow retardation rates are rarely so great that the wake becomes unstable. The boundary layer on an element beneath the wake is nearly always in worse trouble. However, the merging of boundary layers helps establish the optimum. If the boundary layer were much thinner an optimum spacing might be less. Hence, because of scale effects on the boundary layer, the optimum spacing for an aircraft may be appreciably less than indicated by a small scale wind-tunnel model. The problem is worst for the slat because its wake has the longest run.

5. Loads Applied to Boundary Layers by Airfoils

5.1 Introduction

The problem of obtaining high lift is that of developing the lift in the presence of boundary layers—getting all the lift that

is possible without causing separation. Provided that boundary-layer control is not used, our only means of obtaining higher lift is to modify the geometry of the airfoil. Considerations that guide the modification, then, are the subject of this section. It is helpful to think in terms analogous to those of structural design—applied and allowable loads. The airfoil applies the loads, and the boundary layer determines the allowable. Separation of a boundary layer may be likened to reaching the yield point in materials testing. Initial separation rarely coincides with the maximum lift that an airfoil develops, for the lift usually continues to increase. Likewise, the yield point in a metal is not the point of ultimate load. That usually is the rupture point. Hence, the point of maximum lift coefficient may be likened crudely to the rupture point of a material. The analogy is quite rough, of course, but it is mentioned because the interaction between boundary layer and shaping of an airfoil is not very widely appreciated. We close these introductory remarks by observing that aerodynamic science has advanced to the point where we can satisfactorily predict the point of initial separation (the yield point) but not the condition of maximum lift (the rupture point). The second problem is still beyond the state of the art, but it is assuming high priority because of successful solution of the simpler problems.

5.2 Single-Element Airfoils

The subject of single-element pressure distribution types and consequent airfoil performance has been indirectly covered by the material in Sec. 4. The canonical pressure distributions show general limits to the pressure rises, and the pair of charts can be used for visual checks prior to careful examination of more nearly final designs by detailed boundary-layer calculations. If separation is indicated for the problem at hand, some change must be made in the shaping in order to remedy the defect. In making the change, it must be borne in mind that definite bounds on what can be accomplished have already been established. For a one-piece airfoil, there are several possible means for improvement—changed leading-edge radius, a flap, changed camber, a nose flap, a variable-camber leading edge, and changes in detail shape of a pressure distribution. A pressure rise may be improved by changing from convex to concave in the direction of Stratford's type. Even changing the trailing-edge angle from finite (e.g., 10°) to cusp may be useful because a cusped trailing edge imposes less pressure rise at the trailing edge. Furthermore, a cusp increases the slope of the lift curve, so that a given C_L is reached at a lower angle of attack, which lowers nose pressure peaks.

Simple hinge systems as on a plain flap, even though sealed, can have a significant adverse effect on the separation point and hence on lift. Figure 32 shows the adverse effects of the break at a hinge line. The airfoil is an NACA 63A010 airfoil hinged on the lower surface at the 75%-chord point. Also shown for comparison is a variable-camber flap whose centerline is a circular arc. Its final slope is 25°, so that both trailing edges have the same final angle. Both flaps have separation, but the variable-camber shape has attached flow over 85% of the flap, while the simple flap has attached flow over only 71%. It is interesting that the simple hinged flap has a concave pressure distribution and the cambered a convex. In the canonical sense the plain flap pressure recovery is more efficient. The variable camber flap turns out to be better only because of its drastic reduction in the suction peak.

Canonical pressure distributions are useful for preliminary scanning. Figure 33 shows a conventional pressure

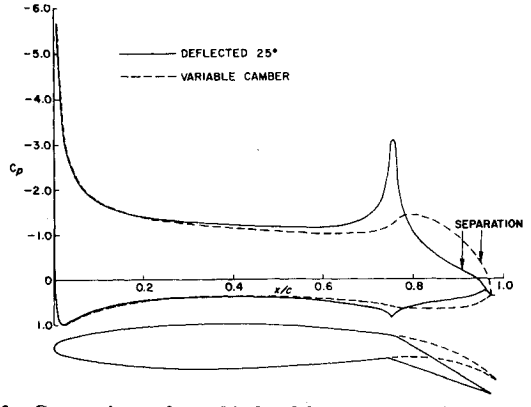

Fig. 32 Comparison of two kinds of flaps on a NACA 63A010 airfoil. For the plain flap $\alpha = 0°$ and inviscid $c_\ell = 1.78$. The airfoil with variable camber flap was set at $\alpha = 1.06°$ in order to obtain the same c_ℓ. Separation points are marked by arrows. $R_c = 10^7$. Transition is at forward suction peak.

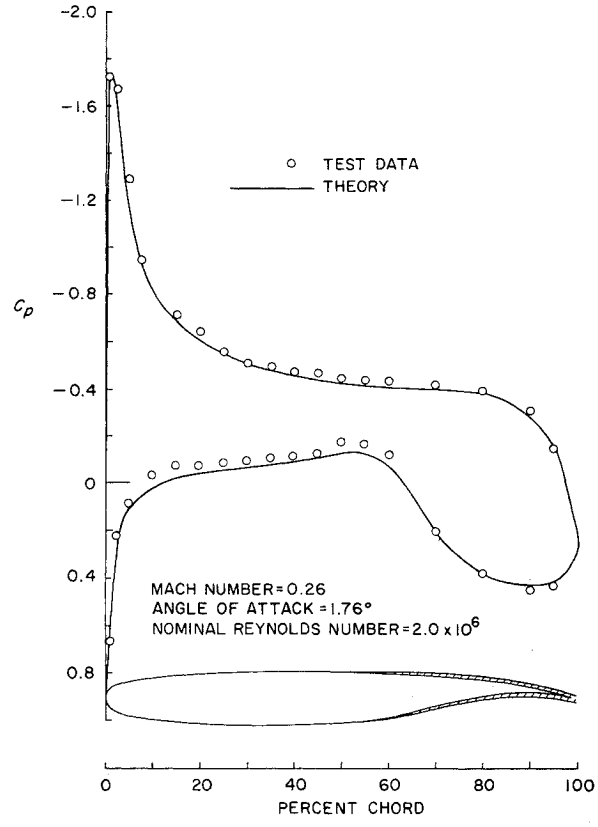

Fig. 33 Pressure distribution for a typical aft-loaded airfoil. Pressure distribution is corrected for boundary-layer effects. The shaded area on the airfoil represents the displacement thickness.

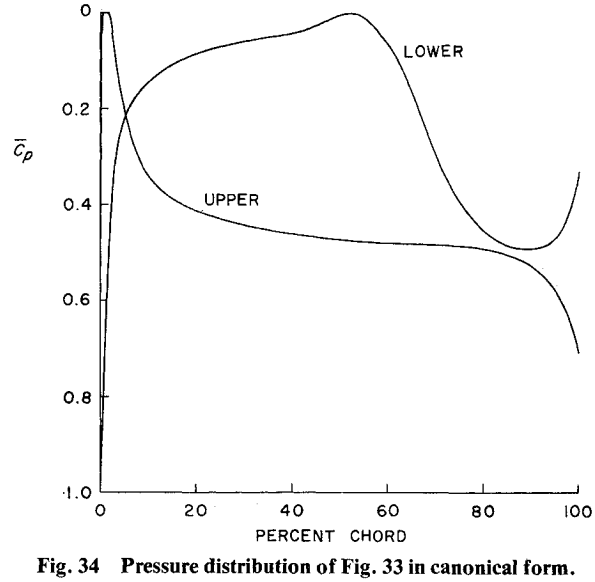

Fig. 34 Pressure distribution of Fig. 33 in canonical form.

distribution. Where is separation most imminent? Near the front on top? Near the rear on top? Or on the bottom? Figure 34 is the canonical form of Fig. 33. Comparison with the curves of Figs. 19 and 20 indicates that the nose is far from separation. The rear upper surface is marginal, but only behind about 97% chord. The lower surface retards to about $\bar{C}_p = 0.5$ in a rather short distance, and the retardation begins late. Figures 19 and 20 indicate that a $\bar{C}_p$-value of about 0.6 could be reached in this distance. Hence there seems to be some margin, but not much. Provided that other constaints would allow it, the faintly S-shaped pressure distribution aft of 50% chord on the bottom could have been improved by replacing it with one that is concave all the way. In problems and approaches like this, the need for inverse methods become evident. First, we would like to have an inverse boundary-layer method that for arbitrary initial conditions could tell us what pressure distribution we could have that contains a certain margin against separation. Then, given the specified pressure distribution, the method should find the airfoil shape that produces it. Definite progress is being made along these lines.

5.3 Multi-element Airfoils—General

There seems to be a great deal of ignorance and confusion about the effect of gaps in properly designed multielement airfoil systems. One misconception was mentioned in the introduction to Sec. 4. The most common misconception is that a slot supplies a blowing type of boundary-layer control. The idea can be traced at least as far back as Prandtl,[33] who said, "The air coming out of a slot blows into the boundary layer on the top of the wing and imparts fresh momentum to the particles in it, which have been slowed down by the action of viscosity. Owing to this help the particles are able to reach the sharp rear edge without breaking away." Abbott and von Doenhoff[34] merely make the safe comment, "Slots to permit the passage of high energy air from the lower surface to control the boundary layer on the upper surface are common features of many high-lift devices." Here again, boundary-layer control is implied. Perkins and Hage[35] make the harmless and noninformative statement: "The air flowing through the slot in Fig. 2-49 [sic] is accelerated and moves toward the rear of the airfoil section before slowing down and separating from the surface." Lindfield, in Lachmann,[7] has a brief paper on the slot effect. Part of the article describes studies by Lachmann, in 1923, who represented a lifting slat by several vortices located near a circle. The circle was then transformed into a Joukowski airfoil. Lachmann's theoretical studies seem to have been largely forgotten and not really appreciated. However, he considered only half the problem—the effect of a slat on an airfoil. He did not consider the effect of the airfoil on the slat. Lindfield's article is correct as far as it goes, but it is not very factual. He points out the need for better analytical methods before the slot effect can be well analyzed. (Now 14 years later, most of the methods are available.)

A remark about the action of slots comes from a recent NASA report[30]: "It is well recognized that the usual function of the slot is that of a boundary-layer control device permitting highly adverse upper surface pressure gradients to be sustained without incurring severe separation. This stabilizing influence results from the injection of the high energy slot flow into the upper surface boundary layer." A still more recent NASA report[36] states, "This leading-edge slat gives the fluid which passes through the gap between the slat and the main airfoil a high velocity. Consequently, a boundary layer which grows on the upper surface of the main airfoil has more momentum than it would have in the absence of the slat."

There are two things wrong with these statements. First of all, the slat does not give the air in the slot high velocity. If anything, it gives the air low velocity. Secondly, the air through the slot cannot really be called high-energy air. All the air outside the actual boundary layers has the same total head. Properly designed and spaced slats are far enough apart that each component develops its own boundary layer under the influence of the main stream, and there is no merging within the slot. Topologically, the process of boundary-layer development is no different from that on a biplane. Subject to their particular pressure distributions, the two boundary layers on a biplane grow, trail off downstream, diffuse, and finally merge. That is just the process for an airfoil system of two or more elements so long as merging does not occur within the slot.

The next paragraphs will elaborate on and confirm what we have just said. There appear to be five primary effects of gaps, and here we speak of properly designed aerodynamic slots.

1) Slat effect—in the vicinity of the leading edge of a downstream element, the velocities due to circulation on a forward element, for example, a slat, run counter to the velocities on the downstream element and so reduce pressure peaks on the downstream element.

2) Circulation effect—in turn, the downstream element causes the trailing edge of the adjacent upstream element to be in a region of high velocity that is inclined to the mean line at the rear of the forward element. Such flow inclination induces considerably greater circulation on the forward element.

3) Dumping effect—because the trailing edge of a forward element is in a region of velocity appreciably higher than freestream, the boundary layer "dumps" at a high velocity. The higher discharge velocity relieves the pressure rise impressed on the boundary layer, thus alleviating separation problems or permitting increased lift.

4) Off-the-surface pressure recovery—the boundary layer from forward elements is dumped at velocities appreciably higher than freestream. The final deceleration to freestream velocity is done in an efficient manner. The deceleration of the wake occurs out of contact with a wall. Such a method is more effective than the best possible deceleration in contact with a wall.

5) Fresh-boundary-layer effect—each new element starts out with a fresh boundary layer at its leading edge. Thin boundary layers can withstand stronger adverse gradients than thick ones.

Those effects will now be explained and discussed in turn at some length. Laminar bubbles, merging boundary layers, and the like may complicate the problem; but when Reynolds numbers are high and at design conditions, such side effects should not be important. Therefore, only conventional boundary-layer effects are considered.

5.4 Slat Effect

Figure 35 displays the slat effect. A slat that is lifting has circulation in the direction sketched in the upper part of the

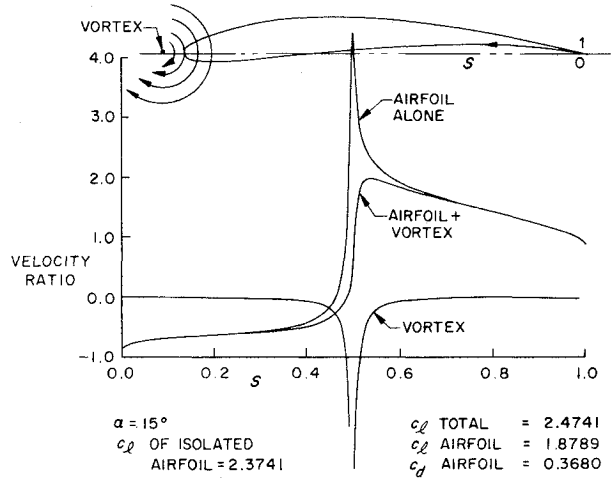

Fig. 35 Velocity distributions on an airfoil with and without a vortex located as shown. S is the arc length around the airfoil surface beginning at the trailing edge, measured in a clockwise direction. Total perimeter is unity.

figure. To a first approximation, a slat may be simulated by a point vortex. A more accurate approximation would account for thickness by means of several sources and sinks, sources in front and sinks behind, the total yield being zero, of course. For our purposes, it is sufficient to consider only the vortex. From the sketch it is evident that the velocities induced on the airfoil by the vortex run counter to those that would develop on the nose of the isolated airfoil, especially at high angle of attack. Pressure peaks would therefore be reduced. Liebeck and Smyth[37] studied the effect by means of a special generalized Joukowski airfoil program combined with computer graphics. Figure 35 is an example of the work. In the method, the vortex could be moved around at will. The best location found for the vortex was typical of the location of a slat. The "best" location is not a precise statement. It is the location where the nose suction peak was largely eliminated and resulting pressure distribution was smooth. At $\alpha = 15°$, the plain airfoil developed a very strong suction peak. As is noted at the bottom of the figure, c_ℓ for the airfoil alone is 2.37. With a vortex located as shown, the pressure peak was completely eliminated, the airfoil c_ℓ fell to 1.88, but the total lift, including the vortex, increased to 2.47. In Fig. 35, the curve called "vortex" shows the velocity induced on the airfoil by the vortex in the absence of the main stream. For best cancellation of the isolated airfoil suction peak, vortex position and strength were so adjusted as to generate a negative velocity peak that was roughly the mirror image of the isolated-airfoil suction peak. Flow near the rear of the airfoil was almost unaffected, as can be seen by examination of either the airfoil pressure distribution or of velocities induced by the vortex.

That then is the slat effect. Contrary to the implication in the various quotations cited in Sec. 5.3, the velocity on the nose of the airfoil is reduced. Peak nose velocity ratio was reduced from about 4.4 to under 2.0. Obviously, the boundary layer is much better able to negotiate the modified distribution. With a vortex operating, there is only a very small increase in total lift, a fact that is consistent with wind-tunnel observations. With slat extended, the main effect is to delay the angle of stall, not particulary to shift the angle of zero lift. In the beginning of this discussion, it was mentioned that thickness effects could be accounted for approximately by sources in front and sinks behind, to approximate the shape of the flap. Since total sink strength must equal total source strength and since the sinks are closest to the airfoil, the net effect of the combination is the induce a small forward velocity component on the airfoil. Hence thickness effects should generally reinforce the circulation effects.

There is an interesting and more physical way of explaining the slat effect. Again consider Fig. 35. When the airfoil is at an angle of attack, flow whips rapidly around its nose, which has a small radius. High centrifugal forces are developed. Without outside help, high negative pressures around the nose are needed to balance out the centrifugal force. But the vortex is a turning aid, and a true slat also would be one. There should be a close correlation between the amount of load carried by the slat and the average C_p-reduction over the nose. The author looked at Fig. 35 and made the following crude estimates: Area modulated = 10% chord, mean C_p of the airfoil alone for this region = −8. Mean C_p for same region with vortex present = −2. Net C_p-change = 6. Then approximate lift force c_ℓ that must be supplied by the vortex is 6×0.6. The actual lift on the vortex is the difference between $c_{\ell_{total}}$ and $c_{\ell_{airfoil}}$. According to the numbers at bottom of Fig. 35, $c_\ell = 0.6$ is indeed the load carried by the vortex. Probably, the analysis cannot be made quantitative, but it does add to the understanding of the flow process. The problem would be a good one for further study. The force exerted by the vortex is not just vertical; it has a drag component too. According to the figure, because net drag must be zero, its c_d-value is −0.3680, a negative force that causes slats to extend automatically. A more careful analysis would consider this component.

The slat effect on a real airfoil is illustrated well by Fig. 36, which represents a well-developed, practical design. The pressure distribution for the airfoil without slat is also shown. The quantity $(u_e/u_\infty)^2$ reached a maximum value of 10.04 ($C_p = -9.04$). With the slat in place, the value was reduced remarkably, to just over 3. The effect is strikingly similar to that of the point vortex in Fig. 35. The figure also shows the upper-surface pressure distribution in canonical form. Again, signs of a jet blowing effect are conspicuous by their absence. This and most of the other pressure distributions were calculated by one version or another of the Douglas Neumann program[38,39] that has been tested by so many hundreds of comparisons with wind-tunnel and other data that its predictions can be accepted as being essentially exact, at least for our current purposes.

Figure 37 was specially synthesized for purposes of this paper. It consists of three identical airfoils, all at the same angle of attack. For comparison and indication of the degree of interference, the pressure distribution for the isolated airfoil is included. Observe the extreme rounding of the peaks of the two rear airfoils, which again is the slat effect. A small amount of the rounding is undoubtedly due to the decreased velocities that accompany a converging flow, as at a trailing edge. As in the point-vortex example, the rear of each airfoil is covered with a surface sink distribution, according to the Neumann program. The surface sinks induce a counter-flow

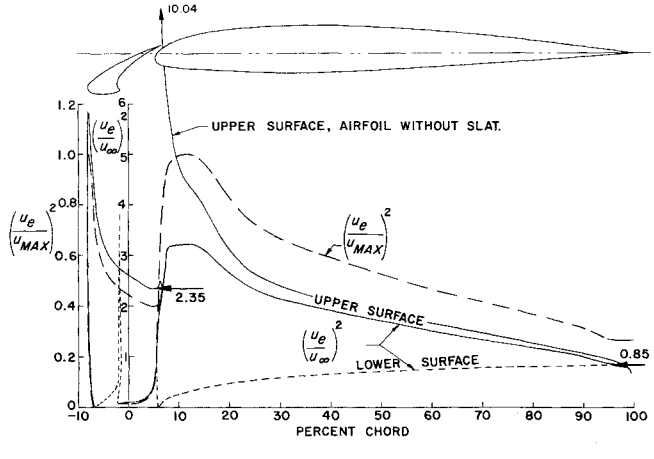

Fig. 36 Typical theoretical pressure distributions for a two-element airfoil, corrected for the boundary layer. The dumping velocity is denoted by the arrows. Also included is the canonical pressure distribution for the upper surface, as well as pressure distribution for the main airfoil alone. The latter exhibits clearly the favorable effect of a slat. $\alpha = 13.15°$, $c_\ell = 1.45$ for the two-element airfoil.

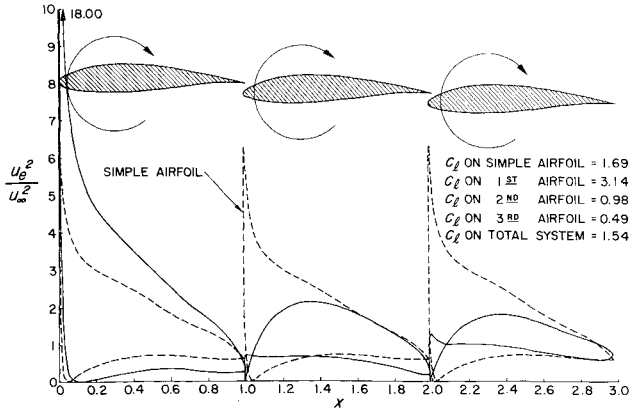

Fig. 37 Pressure distribution on a three-element airfoil formed from three NACA 63_2-615 sections, arranged as shown. All are at the same angle of attack, 10°. Shown also is the pressure distribution on the basic simple airfoil at 10° of attack. Slot gaps are 1% of each chord.

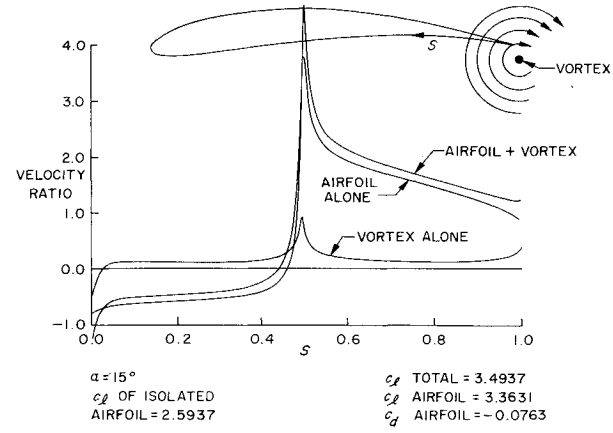

Fig. 38 Point vortex used to simulate a slotted flap. Vortex increases c_ℓ of airfoil at $\alpha = 15°$ from 2.59 to 3.36. Leading-edge pressures are greatly increased by action of the vortex.

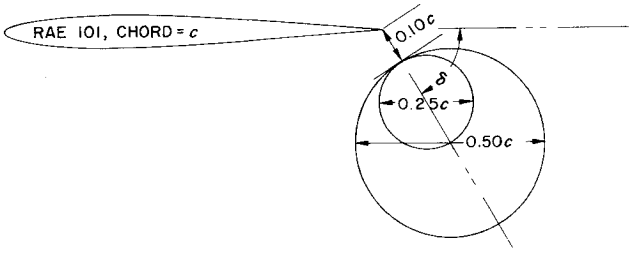

Fig. 39 Airfoil-circular-cylinder combinations studied to learn effect of an obstruction on circulation.

over the following airfoil. Although it was not done, it would be easy to learn the thickness effect by replacing a forward element by a much thinner section while keeping the same mean line.

5.5 Circulation Effect

The slat effect has been recognized before; in fact, it was clearly recognized as far back as 1923 by Lachmann.[7] But the circulation effect does not seem to be explicitly recognized. Figure 38, which shows the effect in its simplest form, was produced by the computer graphic setup used in Fig. 35. Since the vortex could be placed anywhere in the field, it was now placed near the trailing edge, as indicated in the figure. If it were to represent the lift of a slotted flap, the vortex circulation would be as indicated. The flow effectively places the trailing edge at a high angle of attack, and if the Kutta condition is to be met, the circulation must increase. The effect is little different from that of deflecting a small plain flap on the isolated airfoil. In that case, the onset flow would be approaching the rear of the airfoil at a considerable angle. But for Fig. 38 we did not turn the trailing edge; instead, we used a device to turn the flow. Figure 38 shows a slightly different airfoil from that in Fig. 35, but again the angle of attack is the same. The vortex has a drastic effect on circulation, increasing c_ℓ from 2.59 to 3.49. In Fig. 38, the vortex-alone curve shows the velocity distribution around the airfoil that is induced by the vortex. That distribution does not meet the Kutta condition, but the airfoil vortex combination does, of course. It is obvious from the figure that any means of changing the flowfield near the trailing edge would change the lift. Hence, a source, properly positioned, is apt to be as effective as a vortex. The effects on circulation that are due to aft distortions of the flow are then what we call the circulation effect.

According to Fig. 38, the final upper-surface velocity is increased considerably over the upper-surface velocity for the isolated airfoil. Because of the additional velocity caused by adding the vortex to the general translational flow, the airfoil discharges boundary layer at the trailing edge into a stream that is locally of higher velocity. That is the "dumping effect" that has already been mentioned and that will be discussed further in Sec. 5.6.

We have just indicated that any method capable of introducing cross flow at the trailing edge will influence the circulation. An obstruction, properly placed, can be a powerful factor for controlling the circulation. To illustrate such control, we used a circular cylinder, which is about as neutral a body as can be selected. Figure 39 shows the system studied. Two circular cylinders of different diameters are centered on a ray from the trailing edge. The gap is constant at 0.1 chord. The angle of the ray, δ, was varied from 0° to 90°. The lift on the airfoil and on the airfoil-circle combination was calculated. Figure 40 shows some results for the case where the cylinders were directly to the rear of the chord line ($\delta = 0°$). Large increases in lift are indicated. The cylinder itself carries a large amount of lift, even though it has no trailing edge. Figure 41 shows the effects in more detail, as functions of δ. As might be expected, an optimum deflection angle is found. The most effective angle is about 60° or 70°. At 15° angle of attack, the lift coefficient of the isolated airfoil is $c_\ell = 1.75$. With the $0.50c$ circular cylinder set at $\delta = 60°$, $c_\ell = 3.35$ for just the airfoil, nearly double the value for airfoil alone. Hence the effect is very great. Figure 39 is drawn with $\delta = 60°$. It appears that this most effective position is similar to the position found most effective for slotted flaps and slats in combination with airfoils. Considered as a control surface, the control effectiveness $\partial c_\ell / \partial \delta$ is not much less than that of a plain flap.

Figure 42 shows calculated pressure distributions for the cases with $\delta = 60°$ and with c_ℓ held constant at 1.5. The corresponding values of α are noted in the figure. Peak velocities at the nose are considerably reduced by the cylinder. If the pressures were plotted in canonical form, the ones with the cylinder would appear considerably more favorable. Velocity ratios at $0.975c$, which amount to the dumping velocity, are tabulated. The cylinders double the dumping velocity ratio. However, according to Figs. 19 and 20, separation should still occur in all cases. That is not surprising, in view of the specified c_ℓ and shape of the airfoil.

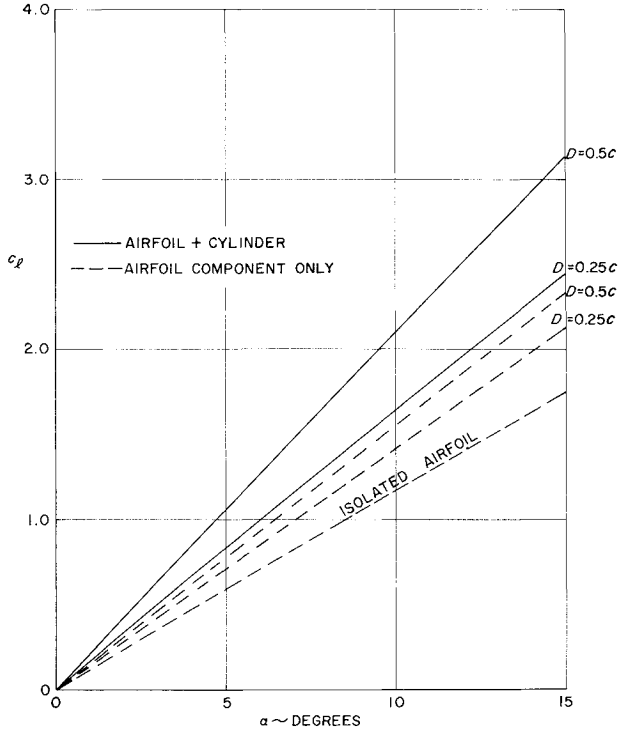

Fig. 40 C_ℓ vs α curves for airfoil-cylinder combinations, showing strong effects on circulation. Deflection δ of cylinder = 0°.

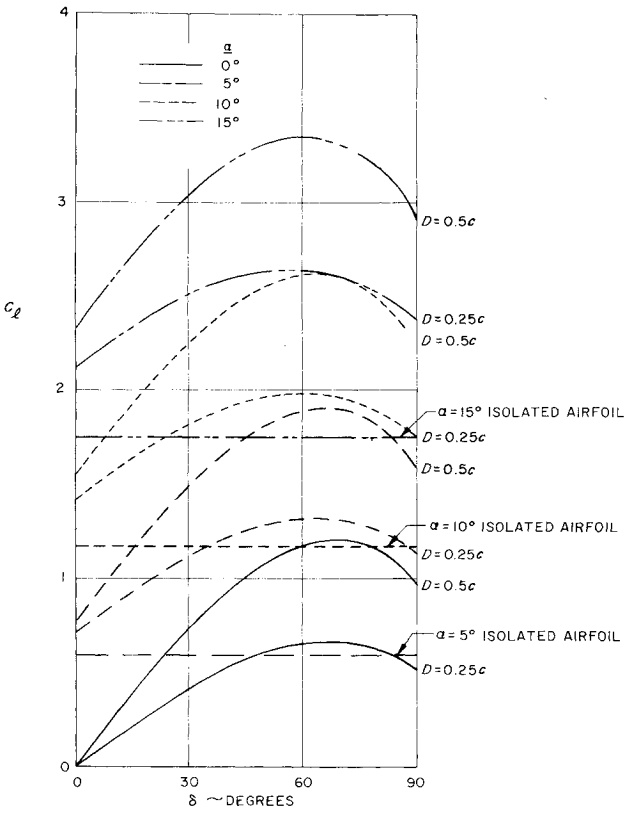

Fig. 41 Airfoil-circular-cylinder combinations. Effect of α,δ, and diameter on lift coefficient.

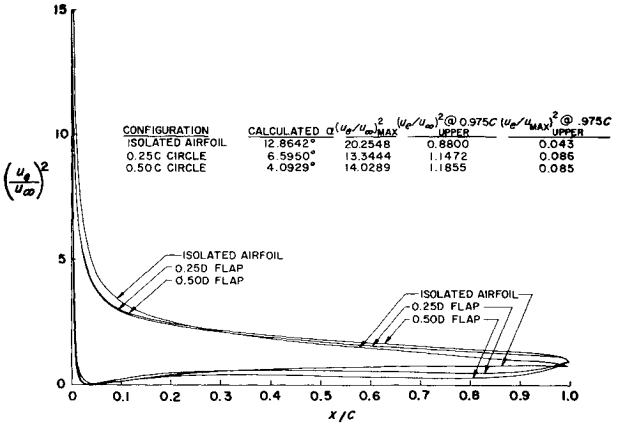

Fig. 42 Pressure distribution at $c_{\mathcal{L}} = 1.5$ for airfoil-cylinder combinations. $\delta = 60°$.

The velocity u_e on the surface of an isolated circular cylinder in crossflow is $u_e/u_\infty = 2 \sin \beta$, where β is angle from the nose. For our problem, the velocity component that is normal to the airfoil is $2 \sin \beta \cos \beta = \sin 2\beta$. The maximum value of that component, which occurs at $\beta = 45°$, is not much less than the $\delta = 60°$ maximum seen in Fig. 41. The rough coincidence justifies the assumption that the change in circulation is a function of the cross flow induced at the trailing edge by other bodies.

Another aid in thinking about the problem of modifying the circulation is to consider the rear stagnation point in nonlifting flow. Without circulation, the rear stagnation point is on the upper surface at some distance forward of the trailing edge. The farther it is moved forward, by whatever means, the greater the circulation required to move it back to the trailing edge. The two guidelines—cross-flow strength and nonlifting stagnation-point location are the best that can be proposed as means of understanding and designing to maximize the circulation. The factors cannot be isolated—there are too many interactions. Fortunately, accurate multi-element-airfoil analysis methods are available, together with much experience. But perhaps factors such as those discussed here will be of value in endeavors to improve design. Rarely do people involved in design of a slotted flap understand why the best place to position the nose of the flap is slightly behind and below the trailing edge of the main airfoil. They just know that with the flap in that position the system worked. We hope we have explained why.

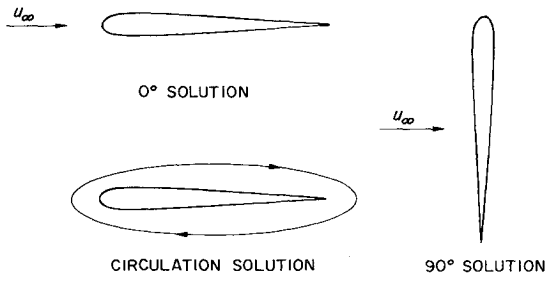

Fig. 43 Three fundamental solutions used for calculating flow about a lifting airfoil at angle of attack.

The reason why augmented circulation is helpful needs to be given. In numerical airfoil methods of the Douglas-Neumann type, the complete solution is a linear combination of three fundamental solutions, which are shown in Fig. 43. Because of the small radius of the leading edge, local velocity ratios in that region are very high indeed for both the 90° and the circulation solutions. A positive lifting circulation is shown in Fig. 43c. It is clear that its disturbance velocities add to those of the 90° solution for positive angles of attack. For an ordinary airfoil, increasing the lift requires increasing the angle of attack. But in the process more of the undesirable 90° solution enters into the summation. Now if the airfoil nose can be kept at low angle of attack, a gain will be made if circulation can be produced by other methods. A plain flap increases that circulation because when it is deflected, a considerable cross-flow component of the onset velocity exists at the trailing edge. The vortex or an obstacle at the trailing edge has the same effect. To avoid nose peaks, the nose should be at a slight negative angle in any real design, in order that the velocities in the circulation and in the 90° solutions oppose each other and cancel out, or more precisely, the linear combination of the three solutions substantially cancels out. In short, considering the separation problem, high lift is best obtained by keeping the nose angle of attack low and inducing circulation by means other than pitching.

Figure 37 illustrates the circulation effect. The c_ℓ on the rear airfoil, which has no device to augment its circulation, is only 0.49. The rear airfoil boosts the circulation of the middle airfoil, which has a c_ℓ of 0.98. The two rear airfoils act together on the front airfoil, giving it a c_ℓ of 3.14. There is some feedback, of course. Circulation on a forward element effectively reduces the angle of attack of a rear element, as well as the velocities on its surface, and hence reduces its lift. That is one reason for the very low lift of the rear element.

In Sec. 4.1, it was suggested that slots amount to a short-circuiting of the lift. That effects seems to exist if the elements are not properly poisitioned. Observe the drop in pressure near the slots in Fig. 37. It is interesting to note that at 10° angle of attack, according to inviscid-flow calculations, the single-element airfoil carries slightly more load than the three-element system.

The same kind of interaction occurs between sails on a sailboat or even between sailboats in close proximity. According to Fig. 37, if the airfoils correspond to sailboats, the last two boats, which are drawing up on the leader, would find it very difficult to pass him. They are augmenting his lift and reducing theirs. The effects are even stronger between

sails on the same boat. A useful and very interesting study of the problem has been made by A. E. Gentry.[40] By using the electrical-analogy technique and conducting paper, he explained correctly for the first time the jib-mainsail interaction effect.

5.6 Dumping Effect

Closely related to the circulation effect is the dumping effect. The favorable interference of a downstream element induces cross flow at the trailing edge that enhances circulation of the upstream element. But the interference may also increase velocities in a tangential direction so that the flow from a forward element is discharged into a higher velocity region, thus reducing pressure-recovery demands. The effect is quite favorable to the boundary layer. According to Eq. (4.4), the suction lift can be increased in proportion to $(u_{T.E.})^2$ for the same margins against separation.

Does the effect really exist? Yes, indeed! It can be seen in any properly designed multielement airfoil. It is clearly shown theoretically in Fig. 42; values of the dumping-velocity ratio are tabulated in the right-hand columns of the table in the figure. For the three cases—plain airfoil, airfoil plus 0.25c circle, and airfoil plus 0.50c circle—the velocity ratios are 0.88, 1.147, and 1.186, respectively. The canonical ratio nearly doubles; it increases from 0.043 to 0.085.

Figure 36 is a theoretical case for an airfoil with slat. For the main airfoil, the dumping-velocity ratio squared is 0.85. On the slat, it is much higher: 2.35. The pressure distributions are also shown in canonical form, and according to them the slat is less severely loaded than the main airfoil—in the sense of margin against boundary-layer separation.

Figure 44 shows experimental data for a three-element airfoil. Again the dumping-velocity effect is clearly displayed, this time confirmed by experiment. For the three surfaces, starting with the flap, the dumping-velocity-squared ratios $(u_e/u_\infty)^2$ are 0.67, 2.0, and 2.28. The canonical plots indicate that, for the conditions shown, the main airfoil is less severely loaded than the slat and the flap. The enhanced dumping velocity shown is typical. The pressure distribution of any properly designed multielement airfoil shows it; one only need look for it.

It is interesting to conjecture what might be done with the effect if an inverse design method for multielement airfoils became available, assuming that the complete airfoil requirements permitted. Start with some desired pressure distribution for a hypothetical three-element airfoil, for example, that of Fig. 45. The basic pressure distribution that we shall use is shown as the dashed line. Then suppose we seek a three-element airfoil that has that canonical pressure distribution for all three elements. Furthermore, assume that the rear element induces a dumping-velocity-squared ratio $(u_e/u_\infty)^2$ of 1.5 on the middle element. Because that element now has higher circulation, it can induce even greater effects on the front element. Assume the induced velocity ratio is the same for each element with respect to its own velocities, which is a bold assumption. With that assumption, the pressure distribution for the three elements in Fig. 45 is as sketched. The load carried is far greater than that of the equivalent single-element airfoil, yet the several canonical pressure distributions are all the same.

The effect, as just described, is readily quantified. It will be done only for a three-element airfoil, but the analysis is easily generalized. Let c = chord of the ensemble; f_1c = chord of rear airfoil (element 1); f_2c = chord of center airfoil (element 2); and f_3c = chord of front airfoil (element 3). Then for the three elements $f_1+f_2+f_3=1$. Also let m_2 = magnification ratio for velocity at trailing edge of element 2 due to being in the high-velocity field of the nose of element 1; and m_3 = magnification ratio for velocity at trailing edge of element 3 due to being in the high-velocity field of the nose of element 2.

Let the upper-surface lift coefficient be c_{ℓ_0} for the given basic pressure distribution. Then for the rear element the suction-side lift is $f_1c_{\ell_0}$. On element 2, the wind speed over the whole element is greater by a factor m_2. Hence for element 2, the lift is $f_2c_{\ell_0}m_2^2$. For the front element, the apparent wind speed is increased by a factor m_3. But the speed on the middle element has already been increased by the factor m_2. Hence on element 3 the lift is $f_3(m_2m_3)^2c_{\ell_0}$. Then the lift of the ensemble is

$$c_\ell = f_1c_{\ell_0} + f_2m_2^2c_{\ell_0} + f_3(m_2m_3)^2c_{\ell_0} \tag{5.1}$$

and the ratio is

$$(c_\ell/c_{\ell_0}) = f_1 + f_2m_2^2 + f_3(m_2m_3)^2 \tag{5.2}$$

For the example of Fig. 45, $f_1=0.30$, $f_2=0.55$, and $f_3=0.15$. Also, $m_2=m_3=(1.5)^{1/2}$. Then, according to (5.2),

$$(c_\ell/c_{\ell_0}) = 0.30 + 1.5(0.55) + 2.25(0.15) = 1.463$$

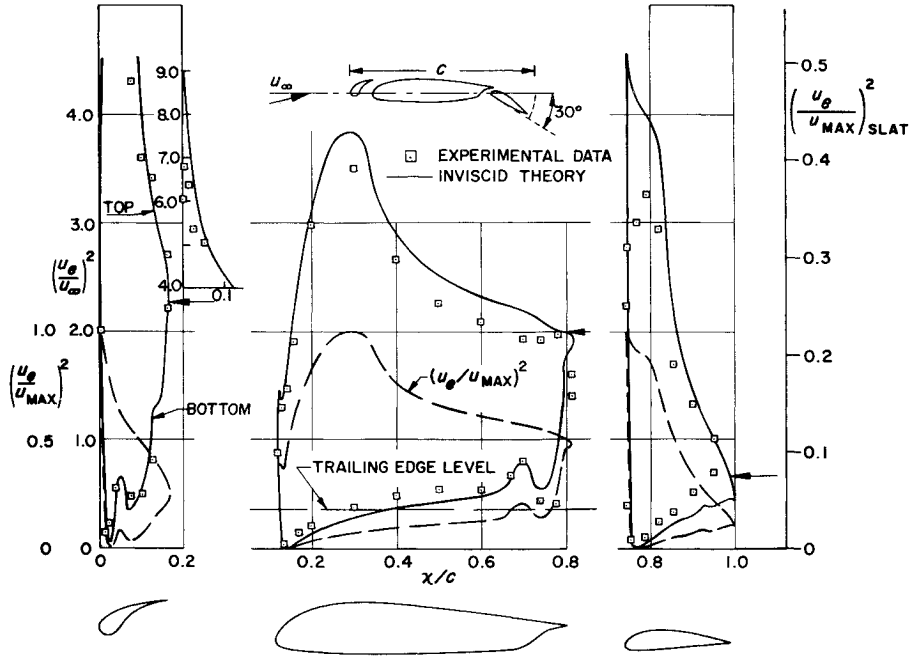

Fig. 44 Typical three-element airfoil, showing dumping velocity effect. Arrows denote dumping velocity. NACA 23012 airfoil, $\alpha=8°$. Line marked trailing edge level is trailing edge dumping velocity divided by maximum velocity on main element.

that is, a 46% gain, with no more tendency for separation than on the base airfoil. The effect definitely exists, but (5.1) is as much hypothesis as it is statement of fact. In any real airfoil design, so many more factors enter into the problem that is is not nearly that simple. Compressibility problems would ultimately set in, for instance.

5.7 Off-the-Surface Pressure Recovery

Off-the-surface pressure recovery has already been discussed in Sec. 4.9. Without its assistance, boundary layers would often be unable to meet all pressure-rise demands. Consider Fig. 44, which represents theory roughly confirmed by test data. The scale on the right-hand side shows the total deceleration ratio from the peak velocity. At the trailing edge of the flap, the velocity-squared ratio has decreased to 0.075. Figure 17 shows a theoretical pressure distribution that can be realized experimentally. Its final velocity-squared ratio is 0.025. According to Figs. 19 and 20, the flow would never have reached such very low velocity ratios if it had been a simple boundary-layer flow that was always in contact with a wall. But in multielement flows, the front element's boundary layer, which undergoes the greatest deceleration ratio, is largely decelerating off the surface. Figure 4 illustrates an airfoil that shows a theoretical total deceleration ratio $(u_{T.E.}/u_{max})^2$ equal to 0.0045.

It is opportune to mention something that has been almost taken for granted—that any accurate calculation of pressure distributions must take into account the displacement thickness of the boundary layer. That assumption is well covered in Ref. 39. In this paper, we have not been consistent, because consistency is not necessary to illustrate our point. In general, our simple theoretical calculations do not consider boundary layers. In other cases, we note in the caption whether or not boundary-layer corrections were included.

A wake alongside a body has only a slight effect on the inviscid theoretical lift. If a wake has a square profile, it can be approximated by sheets of vorticity, positive vorticity on one side and negative on the other. Obviously, the wake has some effect on circulation, although the two sheets almost cancel each other. Furthermore, if the wake flow is curved, there is a centrifugal force of the same sort that is developed by the curved sheet of a jet flap, except that here the momentum amounts to a defect instead of an excess. Foster, Ashill, and Williams,[32] and Ashill[41] have carefully examined those effects in both theoretical and experimental studies. They develop formulas for the various effects. In general, they found that, for properly designed multielement airfoils, the only effect of importance is that of the displacement thickness. Moser and Shollenberger[42] also have studied the problem theoretically and experimentally. They found that the theoretical inviscid effect of the wake is to reduce lift by a small amount, typically a few hundredths in c_ℓ. Their theory is in satisfactory agreement with experiment. In one particular study that used an NACA 4415 airfoil, they found that c_ℓ was reduced by an amount 2.3 c_{ds}, where c_{ds} is the drag coefficient of the slat. All the findings have, in general, been confirmed by practical experience.

To summarize—without the displacement-thickness correction the errors are greater than desirable. With the displacement thickness considered, the errors are so small that a design engineer would hardly know what to do with more accuracy—in the case of fully attached flow, of course.

5.8 Fresh-Boundary-Layer Effect

On each element of a properly designed multielement airfoil, the boundary layer starts out afresh. It is well known, of course, that thinner boundary layers can sustain greater pressure gradients than thicker ones. That fact is demonstrated well by Figs. 19 and 20. It can be displayed in a more analytic form by Stratford's formula, Eq. (4.10), which we here repeat.

$$\bar{C}_p \left[x \frac{d\bar{C}_p}{dx} \right]^{1/2} = (10^{-6}R)^{1/10} S \qquad (4.10)$$

where S is a constant. The term $(10^{-6}R)^{1/10}$ varies so slowly that it is almost constant. But x, a measure of distance from the origin of the flow, enters to the 1/2 power, and, obviously, longer boundary layers admit less adverse gradient. Viewed in another way, we see that if x is halved, $d\bar{C}_p/dx$ can be doubled with the same safety against separation. Therefore, breaking up a flow into several short boundary-layer runs is favorable with respect to the delay of separation and hence to the increase of lift. It might be argued that breaking up the surface into a number of elements steepens gradients just as much as length is shortened, leaving $x(d\bar{C}_p/dx)$ unchanged. In view of the favorable interference and shape of the total pressure distributions the quantity does indeed reduce.

5.9 Are Two Elements Better Than One?

Our previous discussion indicates that several elements are better than one element. But there has been no proof. Here we shall attempt a proof. The proof will be for a two-element case, but by the nature of the development it will be seen that the proof could also show that three elements are better than two, four better than three, etc. We make the following

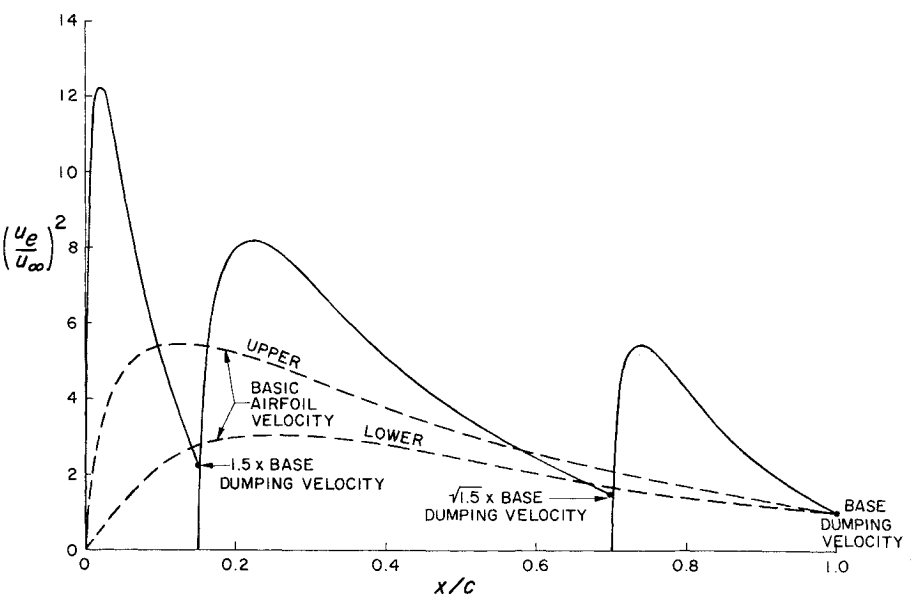

Fig. 45 Illustration of compounding of lift by using multielement airfoils. For this illustration the factor m is $(1.5)^{1/2}$.

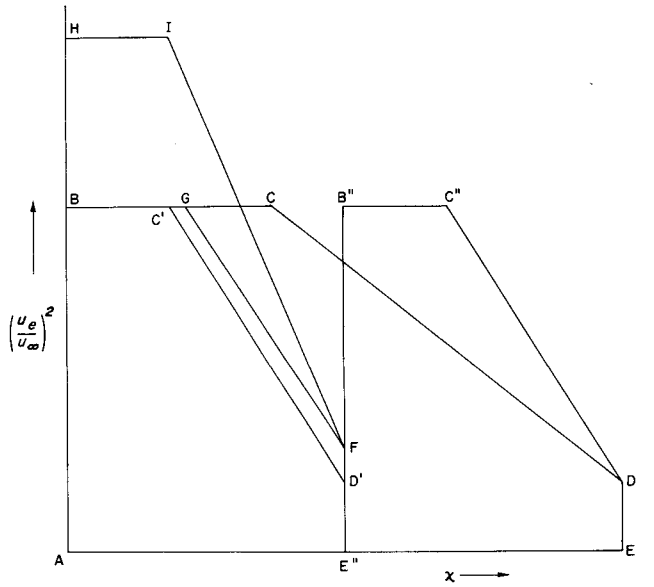

Fig. 46 Load diagram for proof that a two-element airfoil can develop more lift than a single-element airfoil.

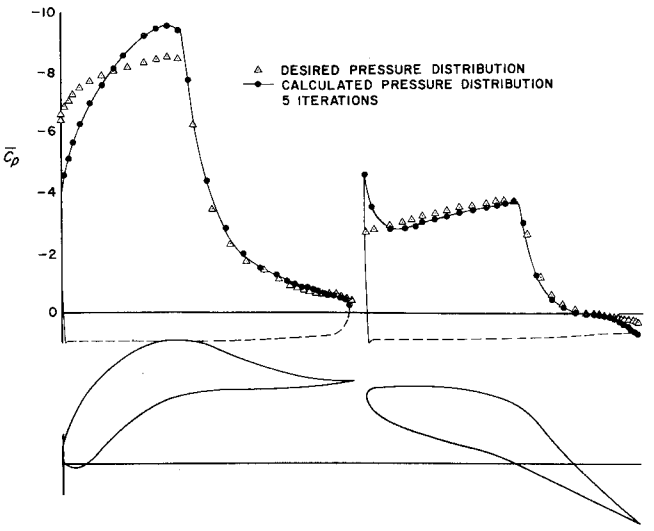

Fig. 47 Shapes producing Liebeck-Stratford pressure distributions similar to that of Fig. 26. Velocity-squared values on the forward element are required to be magnified by a factor of two. c_ℓ of the combination is 3.82.

assumptions: 1) the lower surface plays only a weak role, and hence only the upper surface needs to be considered; 2) Reynolds number effects are weak—which they are at large scale. Hence the lift on an airfoil whose chord is unity is just the same as the lift on two of the same airfoils whose chords are each 1/2; 3) by some means, perhaps an inverse method, the elements can be so shaped that both develop the same canonical upper-surface pressure distribution. The shape of the pressure distribution is not restricted; and 4) boundary layers and wakes of forward elements do not degrade the lifting capacity of following elements.

Consider Fig. 46. Let ABCDE be pressure distribution on the upper surface of an airfoil of chord AE. That same load distribution could be applied twice, to two 1/2-chord elements as loads ABC′D′E″ and E″B″C″DE. The sum of those two areas equals area ABCDE. By proper inverse methods, the shapes of two elements that could generate the same pressure distribution can probably be found, although that is a weak point of our proof. For the two half-size pressure distributions, the basic dumping velocities squared are E″D′ and ED, which are equal. Now on any properly designed multielement airfoil, the flow off the trailing edge of the forward element can be made to discharge into the high-velocity region of the rear element. Hence for the front element the dumping velocity squared is increased from E″D′ to E″F. The increase is the key to our proof. Two cases now arise:

a) the maximum velocity has some kind of limit; and

b) the maximum velocity has no limit.

Consider case (a) first. Perhaps the velocity limit comes from Mach number considerations. Because E″F<E:D′, the start of pressure rise can be moved back from point C′ to a new point G. Now, area ABGFE″ > ABC′D′E″, which proves our case. Consider case (b). If dumping velocity is increased from E″D′ to E″F, the entire forward pressure distribution can be scaled in the ratio E″F/E″D′ to obtain AHIFE″. Again, and even more strongly, area AHIFE″ > ABC′D′E″. Q.E.D.

We have not assumed that the basic canonical pressure distribution be any kind of optimum – just that it be carrying its capacity load without separation. It is not necessary to the proof that the two elements be of equal chord. One possible weakness of the proof is that for a two-element airfoil the final velocity DE cannot be maintained at as great a value as it can for a single-element shape, which means that all pressure levels would be depressed. That is a problem that can best be answered by inverse multielement-airfoil theory, for which there is a great need and a great future.

An attempt to apply these concepts has been made using Wilkinson's approximate multielement inverse method.[43] By means of the method we searched for the shape of a two-element airfoil that had the same thickness distribution and the same canonical upper surface pressure distribution as in Fig. 26. The distributions were to apply to both elements and the dumping velocity ratio of the forward element was to be (2)$^{1/2}$ times that of the rear element so that all u_e^2 values on the front element would be twice those on the rear. Chords of the two airfoils were to be equal. Figure 47 is the result. A drastic change in shape is shown. We obtain a c_ℓ-value of 3.82, compared with 2.31 for the single element airfoil. Because both pressures are identical in the canonical sense, there is no greater danger of separation on the two-element airfoil than on the single-element airfoil. Only one gap size and position was tried. Other gap geometries would change the shape. The method cannot be called entirely satisfactory; partly because of iteration difficulties. It is noticed that the asked for pressure distribution is measurably different from the best that could be found using Wilkinson's method. Whether the asked for pressure distribution is even possible to develop of course is unknown. It is well known that every shape has a corresponding pressure distribution, but not every pressure distribution has a corresponding shape. Nevertheless, the result is indicative of what can be done and of things to expect in the future. It confirms our proof that two elements are better than one.

5.10 Two Spectacular Examples of High-Lift Airfoils

In Sec. 2, Handley Page's 8-element airfoil system was shown (Fig. 4). It occurred to me that it might be of interest to calculate its theoretical pressure distribution, not only to show the power of modern computation but also because it might afford information about interactions, dumping velocity, and other features not clearly exhibited in the usual multielement airfoils that are so strongly hardware oriented; where they are influenced by the requirements of construction and restriction.

Coordinates were measured from a photographic blowup of the illustration in Handley Page's original paper.[5] (It is hoped that his original drawing was accurate.) Figure 4 shows the results. His 8-element shape developed a wing $C_L \simeq 3.3$ at $\alpha = 42°$ (see Fig. 5). The wing was rectangular and had an aspect ratio of 6. According to wing theory, the midspan section was at an effective angle of attack of about 36°, the value used in our two-dimensional calculations. No boundary-layer corrections were made. The total calculated section c_ℓ was

4.33. Velocity ratio instead of velocity ratio squared was used in order to avoid excessively large ordinates on two of the figures (C_p less than -36 was indicated).

Values of c_ℓ in each velocity diagram represent the lift carried by that element, referred to full chord. Four of the diagrams show a second pressure distribution. It is the one that would develop if the airfoil was alone, at the same angle of attack. The leading element is at a considerable negative angle of attack, with a strong pressure peak on the lower side, which might cause separation. Nevertheless, the element is very highly loaded. In spite of the increasing angle of attack of each element, the lift contribution decreases continuously towards the rear. The final element carries a c_ℓ of only 0.08, in spite of being at almost 90° angle of attack at the trailing edge. If it were in isolation, it would be carrying c_ℓ of 6.80.

Although not converted to canonical form, none of the pressure distributions appears to be very close to separation, even that of the front element. Perhaps that is not surprising, for we are showing a condition that represents maximum lift for an airfoil whose chord Reynolds number was about 250,000, making the Reynolds number of each element about 50,000. At such low Reynolds numbers, separation should occur quite early, which makes the theoretical pressure distributions look quite safe when judged by our current high Reynolds number standards.

Figure 5 should be reexamined, now that our calculation has been made. In general, it confirms our conclusion that—if properly designed—the more slots, the better. But the seven-slot configuration is inferior to the six-slot configuration. The reason is not known, but the author suspects it is due to drastic modification of the trailing-edge contours when the eighth element was formed (see Fig. 4). Figure 48 shows the dumping-velocity ratio for each of the elements. There is a rather smooth and definitely continuous increase from rear to front. The rearmost element has a value of about 0.4, and the front element reaches 2.25.

Figure 49 shows the extremes that can be reached in producing special-purpose high-lift airfoils. The section shown was designed by R.H. Liebeck of the Douglas Aircraft Company as a wing for Dan Gurney's Indianapolis-type race cars. The shape is a result of careful direct-method analysis and modification of his optimum airfoil studies. As installed on a racer, the wing is rectangular and of aspect ratio 2.15, with small end plates. The wing was designed theoretically, then built without benefit of wind-tunnel tests, and tested on the racer. At an angle of attack of 14°, tufts used to indicate flow separation remain fully attached and the maximum wing-section c_ℓ is about 5, according to calibrated spring-deflection tests.

In the past few years the word "synergistic" has become popular. Those examples, the proof of Sec. 5.9, the dumping effect discussed in Sec. 5.6, as well as the various test data, all indicate that airfoils properly placed in tandem are fine examples of synergism.

6. Power-Augmented Lift

6.1 General

A few remarks should be made about the subject of power-augmented lift. Power properly applied, as through boundary-layer control, can greatly delay separation and hence increase maximum lift. Powered lift augmentation usually requires pumps and internal ducting, which amounts—at least—to weight and cost complications. There is no doubt that higher lifts can be obtained, but whether they make for a better total airplane system is a moot question. The answer depends on the efficiency of the lift-augmentation system. Here we shall confine ourselves to three studies that touch on the theoretical performance possibilities, together with ideas for improving the overall system.

6.2 Area Suction

The thorough studies reported in Ref. 44 show that turbulent flows with mass transfer can be calculated with nearly as good accuracy as turbulent flows over impervious walls. A generalized eddy-viscosity formula has been developed that is responsible for that accuracy. Therefore, it was felt appropriate here to throw some light on the subject of delaying separation, by considering the theoretical suction requirements. An illuminating procedure is to use the $\bar{C}_p = x^m$ canonical plots presented earlier, in Figs. 19 and 20. Because suction introduces another variable, space does not permit us to present results for all four lengths of flat-plate run. Instead, we consider only the one-foot run, which case may be considered roughly to approximate an airfoil with a flap.

In conventional boundary-layer calculations where a transformed stream function is used, we are given the wall conditions that $f'_w \sim u_w = 0$ (no slip) and $f_w \sim \psi_w = 0$ (impervious wall). Then the problem is to find $f''_w \sim c_f$. In the calculations to be presented, we keep $f'_w = 0$, of course, but seek values of f_w that will maintain an arbitrarily chosen constant $c_f = 0.001$. The altered procedure is just a switch in boundary conditions that is entirely acceptable according to mathematical theory. Some kind of real limiting suction would be found for the special case $c_f = 0$, as in Stratford flows, but because the machine program involves numerical

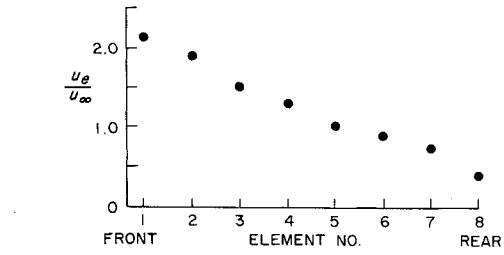

Fig. 48 Upper surface dumping velocity values for the airfoil and conditions of Fig. 4. The ratio $(u_{T.E.}/u_{max})^2$ for the ensemble is 0.0045.

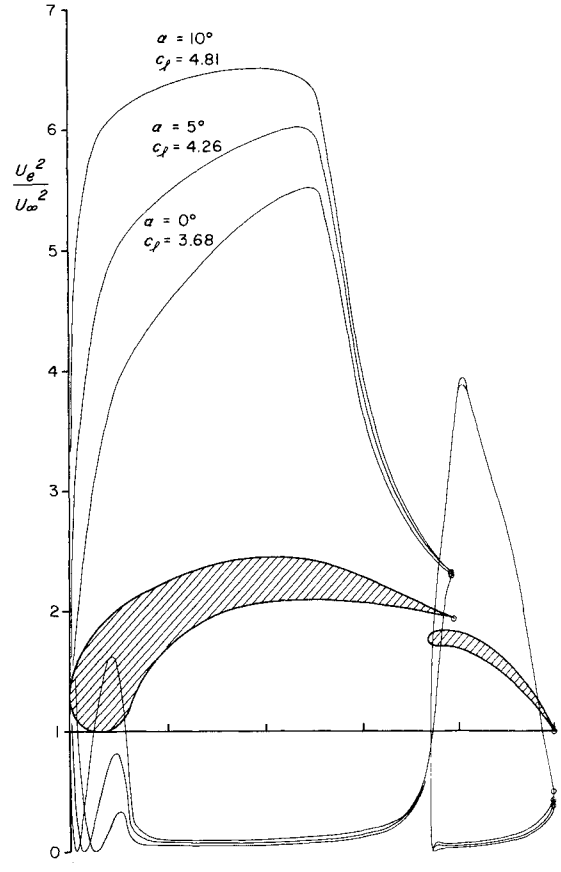

Fig. 49 Special-purpose Liebeck high-lift airfoil designed for Indianapolis-type racers (Pat. Pend.).

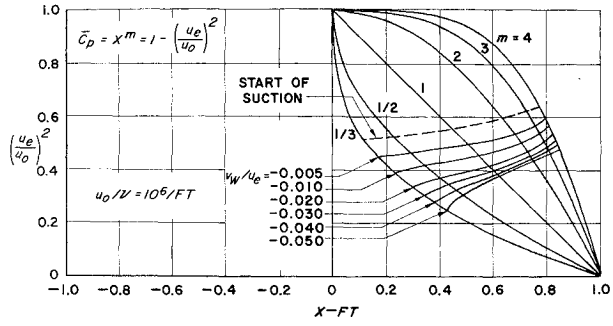

Fig. 50 Effect of area suction on separation. Suction starts where c_f has decreased to 0.001 and then v_w is adjusted to maintain this value of c_f. Initial flatplate run is 1 ft, turbulent, $u_o/v = 10^6$/ft.

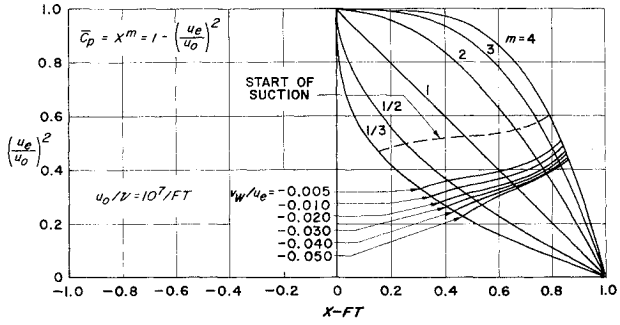

Fig. 51 Effect of area suction on separation. Suction starts where c_f has decreased to 0.001 and then v_w is adjusted to maintain this value of c_f. Initial flatplate run is 1 ft, turbulent, $u_o/v = 10^7$/ft.

solution of a partial differential equation, computing and convergence problems arise when c_f is set equal to zero. We, therefore, avoided those difficulties by specifying that suction would be sufficient to maintain c_f at a value equal to 0.001. Thus the results to be shown contain a certain margin of safety. Previous studies have specified the suction and then found the resulting skin friction. Figures 50 and 51 show results for (u_o/v)—values of 10^6 and 10^7.

The results are shown in terms of values of v_w/u_e required to maintain c_f at the chosen value 0.001. Suction starts where c_f had decreased to 0.001. At first the suction rates are quite small but the rates increase rapidly as the higher pressure region is penetrated. The final contour $v_w/u_e = 0.05$ is one for which a variable constant in the boundary-layer equations is about to exceed the range of its validity. Furthermore, the boundary-layer equations start losing their validity when v_w is not very small compared with u_e. Total suction flow rates can be determined approximately by integrating the v_w values. According to the figures the effect of Reynolds number is not strong.

The charts show that suction is highly effective in causing small delays in separation. But when large delays are desired, suction loses efficiency, so that strong suction is required. The effect can be explained physically in a neat fashion. Assume the region of pressure rise to be quite short so that the suction can be assumed to be concentrated at a point. Let us then examine the special case of a flat-plate flow entering a sudden pressure rise assisted by suction. Long ago, in connection with Griffith airfoils, G. I. Taylor considered the same kind of problem. He first assumed that the pressure rise occurred in such a short distance that the total head along each streamline in the boundary layer would remain constant. Then he hypothesized that no filament whose total head was less than the downstream static pressure could flow into the downstream region of higher pressure. In other words, unless it was sucked off the filament would separate. These hypotheses give us a procedure for calculating the amount of suction required to prevent separation at a pressure jump. His analysis has been well confirmed by experiment for laminar flows, some of the confirmation being the author's.

Let us apply the hypotheses to our problem, namely the flows illustrated in Figs. 50 and 51, except that the pressure rise region will be approximated by an instantaneous jump. Let $(\,)_c$ designate critical conditions. Then, using our canonical flow notation we have for the total head along any streamline

$$H = p_o + \tfrac{1}{2}\rho u^2 \tag{6.1}$$

If all velocity head is expended in reaching a higher pressure, p_c, downstream, we have

$$H_c = p_c = p_o + \tfrac{1}{2}\rho u_c^2 \tag{6.2}$$

where u_c is the velocity of the dividing streamline, all fluid below being sucked off. Using $\bar{C}_p = (p - p_o)/(1/2)\rho u_o^2$ we find

$$\bar{C}_p = u_c^2/u_o^2 \tag{6.3}$$

This relation states that removal of fluid up to a height u_c will permit a canonical pressure rise from $\bar{C}_p = 0$ to $\bar{C}_{p_c}$.

How much flow must be removed? Because the initial flow is flat plate it is convenient to use the 1/7 power formulas. The quantity that must be removed is $Q_c = \int_0^{y_c} u\,dy$ which in coefficient form is

$$C_{Q_c} \equiv \frac{Q_c}{u_o x} = \frac{1}{x}\int_0^{y_c} \frac{u}{u_o}\,dy \tag{6.4}$$

The 1/7 power formulas are

$$u/u_o = (y/\delta)^{1/7} \text{ and } \delta(x) = 0.37x/(u_o x/\nu)^{1/5} \tag{6.5}$$

Upon insertion of the first, and integrating we have

$$C_{Q_c} = (7/8)(\delta/x)(y/\delta)_c^{8/7} \tag{6.6}$$

From Eq. (6.3) and the first of Eq. (6.5) we can also write

$$\bar{C}_{p_c} = (y/\delta)_c^{2/7}$$

When this, together with the second of Eq. (6.5) are substituted into (6.6) we obtain

$$C_{Q_c} = [0.324/(u_o x/\nu)^{1/5}]\bar{C}_{p_c}^4 \tag{6.7}$$

This formula shows that if the demanded pressure rise is indeed low the required suction C_{Q_c} is very low. If $u_o x/\nu$ is 10^7 then $C_{Q_c} = 0.013\ \bar{C}_{p_c}^4$. If $\bar{C}_{p_c} = 0.5$, the required C_{Q_c} is only 0.0008 but for reaching stagnation pressure it is 0.013. Unlike the results on Figs. 50 and 51 some suction is indicated for even the smallest pressure rise, but the fourth power variation shows the demand to be exceedingly small. The most interesting result from this analysis is the fourth power relation of C_Q to $\bar{C}_p$.

In Lachmann,[7] Wuest presents theoretical studies made by Pechau's approximate method. The studies were of area suction applied to simple airfoils in various ways. Suction requirements for avoiding separation are given. Generally, our calculations show the same $C_Q = Q/u_o x$ magnitude as his, that is, of $0(10^{-3})$. We have not presented specific examples, because charts like Figs. 50 and 51 are more general. For a real engineering problem, since the boundary-layer computing method is entirely general, the particular case should be and can be studied carefully. Charts are then just a guide for preliminary estimation purposes.

The results shown represent no kind of optimum. The start of suction was arbitrarily chosen, and the intensity chosen was

such as to maintain c_f at a value 0.001. A smaller c_f-value would clearly reduce v_w and C_Q. In the belief that earlier suction would be slightly less efficient, we started suction only when the boundary layer began needing help. Undoubtedly, there is an optimum distribution for each of the $C_p = x^m$ distributions, but we believe our values do not miss the optimum by very much.

There surely is some best combination of suction distribution and pressure distribution for obtaining the greatest pressure rise with the minimum C_Q. Determining that combination amounts to a calculus-of-variations problem of finding the best combination of path and suction. It is interesting to note that the basic tool for the problem has recently been developed.[45] The boundary-layer calculation method has been extended to find the pressure distribution necessary to provide a given c_f-history, which amounts to solving a nonlinear eigenvalue problem, where the eigenvalue is dp/dx. Since suction could already be analyzed by both direct and inverse methods, we now have available the tools for seeking the optimum combinations of $v_w(x)$ and $p(x)$. The problem is an interesting mathematical challenge.

6.3 Tangential Blowing

To round out the discussion, we give a limited comparison of blowing applied to the same $\bar{C}_p = x^m$ flows. The wall-jet method of Gartshore and Newman[46] is used. As for the suction case, blowing is assumed to start shortly before natural separation would occur, that is, at the $c_f = 0.001$ locus. Figures 52 and 53 are the results.

The conventional blowing coefficient C_μ is defined for two-dimensional incompressible flow as

$$C_\mu = \text{thrust}/qc = (2u_j^2/u_\infty^2)t/c \tag{6.8}$$

When applied to a family of canonical pressure distributions, both reference velocity and reference length lose their meanings. But we know, from basic boundary-layer theory and from the parabolic nature of the equations, that the direct determinants of the development of a flow subject to a certain pressure history are the characteristics of the boundary layer at the starting station. The length of prior run, the pressure distribution, and whether it is laminar or turbulent, only help to establish the boundary layer at the station where the blowing studies are started. When the boundary layer is viewed in this fundamental way, chord and freestream conditions lose their significance. Momentum thickness at the slot comes forward as the logical reference length. Furthermore, the momentum defect at this point is $\rho u_e^2 \theta$, which is a drag force. The tangential blowing produces a thrust. We therefore introduce a new form of the incompressible blowing coefficient called $C_{\mu\theta}$, which is defined as

$$C_{\mu\theta} = \frac{\text{jet thrust}}{\text{momentum defect}} = \frac{\rho u_j^2 t}{\rho u_e^2 \theta} = \frac{u_j^2 t}{u_e^2 \theta} \tag{6.9}$$

Equations (6.8) and (6.9) can be combined to give a relation between the two blowing coefficients,

$$C_\mu = 2(u_e^2/u_\infty^2)(\theta/c)C_{\mu\theta} \tag{6.10}$$

With $C_{\mu\theta}$ as our blowing parameter, we obtain a direct "feel" for the strength of the blowing, for we are making up for the momentum lost in the boundary layer. Then, if the blowing is to be applied over only a short distance, it is to be expected that the required value of $C_{\mu\theta}$ will not be greatly different from unity.

That is indeed the case with Figs. 52 and 53. Gartshore's program deck was used for the calculations. Several different values of u_j/u_e were tried and results were found to be sensitive to the ratio. Furthermore, since the method was only approximate, hangups were encountered in some cases when the

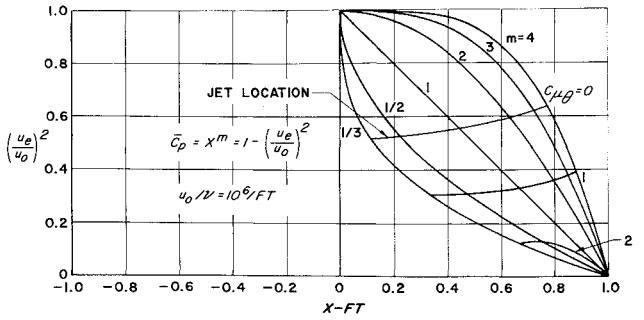

Fig. 52 Effect of tangential blowing on location of separation. Blowing slot is located at point where $c_f = 0.001$. Blowing velocity ratio $u_j/u_e = (10)^{1/2}$. Initial flat plate run = 1 ft, turbulent; $u_0/\nu = 10^7$/ft, Gartshore-Newman type of calculation.

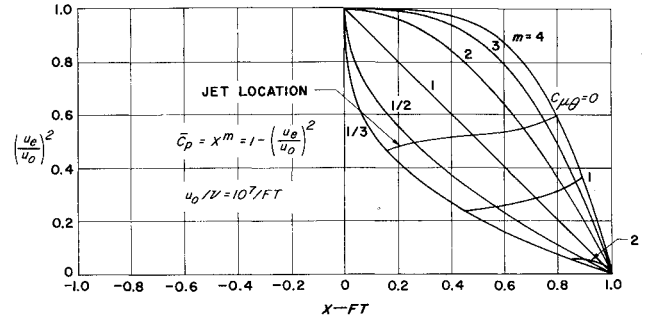

Fig. 53 Effect of tangential blowing on location of separation. Blowing slot is located at point where $c_f = 0.001$. Blowing velocity ratio $u_j/u_e = (10)^{1/2}$. Initial flat-plate run = 1 ft, turbulent; $u_0/\nu = 10^7$/ft, Gartshore-Newman type of calculation.

wall-jet boundary-layer profile developed a hollow. Hence, the values shown in Figs. 52 and 53 should not be considered much more than estimates, or a start toward more precise analysis. The blowing slot is located at the $C_{\mu\theta} = 0$ line, which is the $c_f = 0.001$ locus. Then, as blowing is increased, separation is delayed to the contours noted. Blowing with an intensity $C_{\mu\theta} = 2.0$ appears to delay separation nearly to the stagnation point. Blowing at the $c_f = 0.001$ line with a $C_{\mu\theta}$-value of 1.0 is just enough to make up for the momentum loss at the slot location. Hence the separation locus should be approximately the same as for the case of natural separation when the initial boundary layer is very thin. If one examines Figs. 19 and 20 for the flat-plate run equal to 1/64 ft, he sees that separation locus is not much different from the $C_{\mu\theta} = 1$ loci in Figs. 52 and 53.

6.4 Inverse Problem for Jet Airfoils

A kind of lifting efficiency can be defined for airfoils. It is illustrated in Fig. 54. The efficiency is simply the ratio of the area contained within the canonical-pressure-distribution loop to that of the circumscribed rectangle. The falloff in pressures toward the rear on the upper surface is necessitated

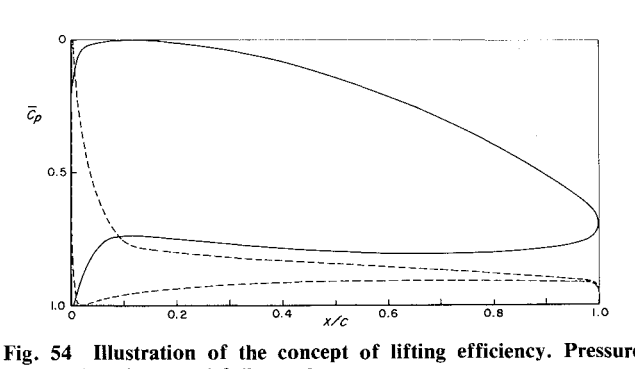

Fig. 54 Illustration of the concept of lifting efficiency. Pressure distributions for two airfoils are shown.

to varying degrees by flow-separation requirements. If the figure represented were a design pressure distribution for some problem, the upper $\bar{C}_p$ bound might be determined by Mach number, for example. Two pressure distributions are shown in Fig. 54, one for a slightly cambered airfoil at angle of attack, the other for a cambered Joukowski airfoil. The cambered airfoil has the higher efficiency. Obtaining lift by angle of attack, according to the definition of efficiency, is inefficient. Because the start of pressure rise can be delayed more if design lifts are low, the efficiency at low lift coefficients is often higher than that of shapes either designed for or operating at high lift.

Powered lift can improve the efficiency markedly. When there is a curved jet, load can be carried by the jet, and it becomes possible to carry load all the way to the trailing edge. Thus the pressure-recovery problem can be eliminated entirely.

A highly accurate theory of jet-flap airfoils that makes it possible to realize that benefit has been worked out in the past few years by Lopez and his co-workers.[47,48] One of his coworkers, Halsey,[48] reviews the airfoil work in general. But here we feel we have space only to mention one aspect of it, a method that appears to have produced an interesting and significant advance. He has developed an inverse method for jet airfoils. That is, the method specifies the pressure distribution and the jet momentum coefficient and finds the airfoil shape and the jet leaving angle necessary to generate that shape.

The method is not a classical inverse method, such as James has developed for conventional airfoils. Instead, it is a kind of iterative procedure that involves finding a mean line and obtaining modified shapes until convergence is reached. Recourse can be had to the exact direct method for checking purposes. The effects of jet entrainment on the pressure distribution are accounted for approximately. The procedure has been found to produce rapid convergence and accurate results. We can do no better than to quote from Ref. 48 to show the specific steps that are taken in finding a shape. The steps, slightly paraphrased, are as follows:

1) Specify the desired airfoil velocity distribution and jet momentum coefficient.

2) Divide the velocity distribution into symmetric and antisymmetric components.

3) Determine the approximate jet-entrainment effects. Since the operation is noniterative, the sink distribution representing the jet is placed on an extension of the airfoil chord, and its strength is determined by assuming that the velocity just outside the jet is equal to the freestream value. The entrainment effects at the true airfoil surface are assumed to be the same as those calculated at the airfoil chord line.

4) Use an inverse method to find the thickness distribution that corresponds to the symmetrical component of the velocity specified in step 2 that remains after entrainment effects have been subtracted out.

5) Design the mean line needed to produce the antisymmetric portion of the velocity distribution, including the influence of the jet. For that purpose, a linearized method is used. This part of the design procedure is the only part that is fundamentally different from conventional design methods. For more details, see Ref. 48. Either: a) the vorticity at the trailing edge can be specified, find the jet angle; or b) the jet angle can be specified, find the vorticity at the trailing edge.

6) Combine camber and thickness distributions.

7) Using the general nonlinear direct jet-flap airfoil method, check the result. If necessary, repeat the cycle with pressures slightly modified to correct errors revealed by the direct-method check.

We present two figures to show typical results. Figure 55 shows the effect of blowing. High blowing rates relieve the camber, assuming that the velocity distribution is maintained constant. The points are checks of the computed inverse shape by means of the direct, nonlinear method using it as input data. The difference in c_ℓ noted for the three airfoils is due to the lift component of the jet. Each airfoil is shown at the angle required to develop the design pressure distribution.

An extreme case, one that taxes the linearized camber treatment, is shown in Fig. 56. Here entrainment effects have been included in the inverse method. The entrainment effects, as well as the entire camber-shape solution, are worked out

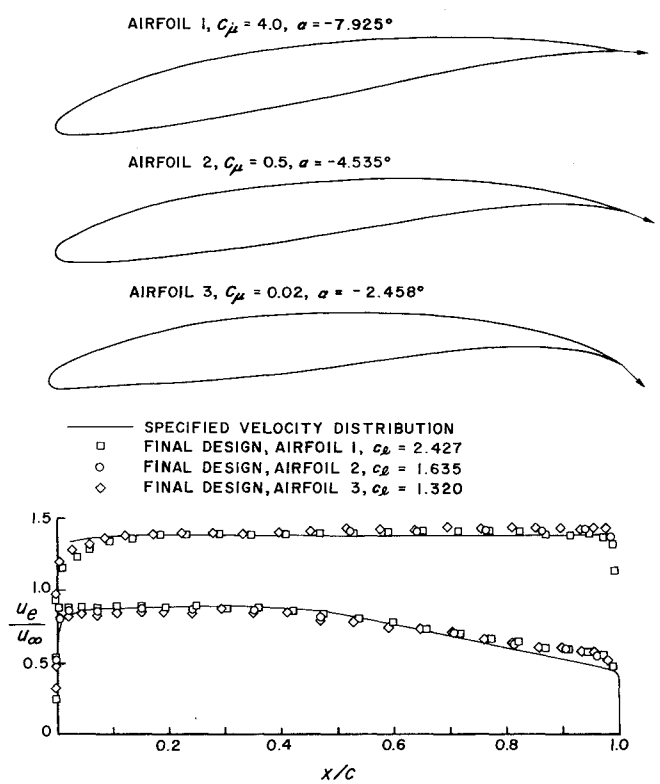

Fig. 55 Effect of C_μ on shape of airfoils all designed to have the same upper-surface velocities. Blowing is in direction of mean line at the trailing edge, and indicated by the arrows. Each airfoil is shown at its design angle of attack.

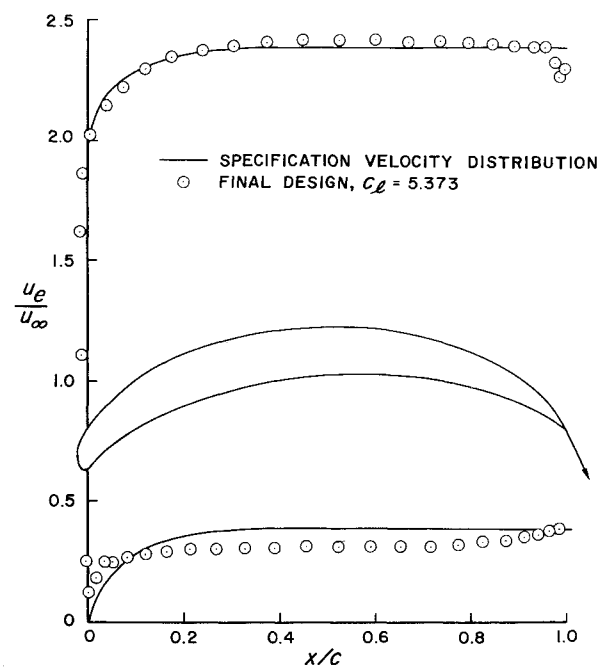

Fig. 56 A highly cambered jet-flapped airfoil designed by the inverse method, including entrainment effects. The solid line is the specified velocity distribution. The o points show check results from the exact nonlinear direct method of calculation.

along the chord line. The final jet angle is at an inclination of $-74.4°$ to the chord plane, and the airfoil is nose down 4.7° to develop the design pressure distribution. Agreement between the exact check calculation and the linear design method is fair. Considering the extreme nature of this problem, the result is satisfactory.

7. The Future

It was my original intention in planning this lecture to devote considerable attention to the state of knowledge about three-dimensional flows and high-lift flows in the transonic region. However, I shall not, for two reasons. First, I am already exceeding the desired length for this paper, and second, there is not much in the way of theory and analysis methods that can be called solid. Low-speed, two-dimensional airfoil high-lift theory has become a fairly "hard" science, but three-dimensional and transonic theory is still no more than a "soft" science, if that much.

It is only necessary to read Callaghan's AGARD lecture notes [19] to realize the diversity of problems that arise as we come closer to real aircraft configurations and to realize the kind of practical empiricism that one is forced to use in applied aircraft design.

Like the two-dimensional problem, the three-dimensional is an analysis involving a combination of inviscid- and boundary-layer flow. The inviscid analysis is nearly here. That is, lifting inviscid-potential-flow solutions can now be calculated readily for as many as 1000 coordinate points. That number will easily solve nearly any simple wing-alone geometry and is rather good at handling wing-fuselage combinations. 1000 points is marginal for a two-element wing alone, but it can produce useful information. To handle three-element wings together with major body effects at least 2000-point solutions are needed. In a private communication, we learn from Norman Donaldson that Bell Aircraft has extended the method to handle 3000 data points. The work is done on a modified UNIVAC 1108 computer. A problem of this size requires more than two hours of machine time. It is hoped that cost per data point continues to decrease.

The boundary-layer solution lags behind the inviscid-flow solution. Although there are formulations and methods for analyzing three-dimensional laminar and turbulent flows—and even a book [49] on the subject—none is powerful enough to analyze the complicated problems of applied analysis that occur, for example, those of swept wings. Progress in fundamental work is encouraging, however. It appears that extensions of the eddy-viscosity formulations used quite successfully for two-dimensional flows do not lose accuracy when extended to three-dimensional flows. [50] In the case of turbulent flow, much empiricism is involved, and the accuracy of a method can be determined only by extensive comparison with experiment. A milestone in the development of the art of computing two-dimensional turbulent boundary layers was the Stanford Conference, [51] in which each participant who claimed to have a good boundary-layer method was asked to calculate a large variety of flows, all from standardized input data under prescribed rules. Sometime in the rather distant future, that kind of conference will be needed to establish the accuracy of methods of calculating three-dimensional flow.

Beyond that problem is the problem of calculating maximum lift, as contrasted with the problem of calculating initial separation. If the calculations of three-dimensional boundary layers are forced to stop when the first separation is encountered, they are likely to do more than barely start. In two dimensions, we can now predict separation reasonably well. With that problem out of the way, the problem of predicting flows with partial separation comes to the front. Ideas being explored range all the way from direct numerical attempts at solving the complete Navier-Stokes equation to approximating the separated region by an inviscid flow.

In the transonic regime, where separation involves shocks, again there is no method of prediction that can be called general. There is a large traffic in papers on shock-boundary-layer interaction, but so far as the author knows, the problem has not been solved in any general sense. A vigorous attack is under way that uses finite-difference methods. Possibly practical methods of analysis will result.

One could talk indefinitely about other special problems related to high lift but that won't do, so I shall end by listing what I think are the ten most important basic theoretical problems of high-lift aerodynamics:

1) Very general calculation of three-dimensional laminar and turbulent flows.

2) Calculation of flows involving partial separation in the rear.

3) Practical calculation of flows involving forward separation bubbles.

4) Practical calculation of flows involving shock-boundary-layer interaction.

5) Calculation of the viscous flow on airfoils and bodies of revolution of length c from about $0.95c$ to $1.05c$. In that region of very rapid change and strong interaction, boundary-layer equations do not apply. With our recently acquired ability to calculate well the forward 95%, our inability to solve the next 10% is a real irritant. Beyond 105% chord, we again can usually do an acceptable job.

6) Further development of inverse methods.

7) Drag of multielement airfoil systems. Drag predictions have a relative error one order of magnitude greater than that of lift predictions. Since propulsive and acceleration information is crucial to aircraft design, that is a very important problem.

8) Practical calculation of merging boundary-layers, wall jets and wakes. Although methods have been developed, it is felt that considerable further development is needed.

9) The analysis of flows over swept wings on which a leading-edge vortex is developed. When the vortex develops, conventional calculations are about 100% in error.

10) Three-dimensional transonic calculations, particularly for arbitrary wings and wing-body combinations.

In several of those problems, the first phase is two-dimensional analysis, but as soon as that is accomplished the three-dimensional looms up as the next target.

As you can see from the list, aerodynamics still has a long way to go before we can truly calculate, instead of just estimate. Yet in retrospect, we see that we have progressed a long way toward the goal in the past thirty years. Perhaps another Wright Brothers lecture should be given on this same subject 20 to 30 years from now. With the computer revolution that we have, the prospects of finding practical calculation methods for most of the ten problems are bright. We hope there will be some new "inventions" in flow and flow control. Cornish's spanwise blowing [52] might be one, and effective application of the trapped-vortex idea [53] might be another.

In October 1908, at a banquet in his honor in France and after very successful flights in September, Wilbur Wright was unexpectedly called on to say a few words. He said, "I know of only one bird, the parrot, that talks, and it can't fly very high." I, too, cannot fly very high and I have talked too much.

References

[1] Prandtl, L., "Über Flüssigkeitsbewegung bei sehr kleiner Reibung," III International Mathematiker-Kongress, Heidelberg, 1904.

[2] Weyl, A. R., "High-Lift Devices and Tailless Airplanes," *Aircraft Engineering*, Oct. 1945, p. 292.

[3] Hagerdorn, H. and Ruden, P., "Wind Tunnel Investigations of a Wing with Junkers Slotted Flap and the Effect of Blowing Through the Trailing Edge of the Main Surface over the Flap," RAE Translation No. 442, Dec. 1953, Royal Aircraft Establishment, Farnborough, England.

[4] "Experiments on Models of Aeroplane Wings at the National

Physical Laboratory," R&M No. 110, March 1914, Aeronautical Research Council, London.

[5]Page, F. H., "The Handley Page Wing," *The Aeronautical Journal*, June 1921, p. 263.

[6]Glauert, H., "The Handley Page Slotted Wing," R&M No. 834, Mar. 1922, Aeronautical Research Council, London.

[7]Lachmann, G. V., *Boundary Layer and Flow Control*, Vol. 1, Pergamon Press, London, 1961.

[8]LePage, W. L., "Further Experiments on Tandem Aerofoils," R&M No. 886, May 1923, Aeronautical Research Council, London.

[9]Harris, R. G. and Bradfield, F. B., "Model Experiments with Variable Camber Wings," R&M No. 677, June 1920, Aeronautical Research Council, London.

[10]Fowler, H. D., "Variable Lift," *Western Flying*, Nov. 1931, p. 31.

[11]Weick, F. E. and Platt, R. C., "Wind-Tunnel Tests of the Fowler Variable-Area Wing," Tech. Note 419, May 1932, NACA.

[12]Alston, R. P., "Wing Flaps and Other Devices as Aids to Landing," *Journal of the Royal Aeronautical Society*, Vol. 39, 1935, p. 637.

[13]Young, A. D., "The Aerodynamic Characteristics of Flaps," R&M No. 2622, 1953, Aeronautical Research Council, London.

[14]Duddy, R. R., "High-Lift Devices and Their Uses," *Journal of Royal Aeronautical Society*, Vol. 53, 1949, p. 859.

[15]Cleveland, F. A., "Size Effects in Conventional Aircraft Design," *Journal of Aircraft*, Vol. 7, Nov.-Dec. 1970, pp. 483-512

[16]Faulkner, S. M., Hess, J. L., Smith, A. M. O., and Liebeck, R. H., "Charts and Formulas for Estimating Velocity Fields in Incompressible Flow," Rept. LB 32707, July 1968 (AD 772 233), McDonnell Douglas Corp., Long Beach, Calif.

[17]Mayer, J. P., "A Limit Pressure Coefficient and an Estimation of Limit Forces on Airfoils at Supersonic Speeds," Research Memo. L8F23, 1948, NACA.

[18]Smith, A. M. O., "Aerodynamic Lifting Potentialities of Aircraft in Subsonic Flight, Rept. ES 20930, 1947, Douglas Aircraft Co., Long Beach, Calif.

[19]Callaghan, J. G., "Aerodynamic Prediction Methods for Aircraft at Low Speeds with Mechanical High Lift Devices," AGARD Lecture Series No. 67, May 1974, von Karman Institute, Brussels, Belgium.

[20]Smith, A. M. O., "Aerodynamics of High-Lift Airfoil Systems," *Fluid Dynamics of Aircraft Stalling*, AGARD-CP-102, 1972.

[21]Assessment of Lift Augmentation Devices," AGARD Lecture Series No. 43, AGARD LS-43-71 (Available as AD 720-259, 1971).

[22]Thain, J. A., "Reynolds Number Effects at Low Speeds on the Maximum Lift of Two-Dimensional Aerofoil Sections Equipped with Mechanical High-Lift Devices," *Quarterly Bulletin National Aeronautical Establishment*, Ottawa, Rept. DM/NAE, 1973.

[23]Cebeci, T., Mosinskis, G. J., and Smith A. M. O, "Calculation of Separation Points in Incompressible Turbulent Flows," *Journal of Aircraft*, Vol. 9., Sept. 1972, p. 618-624.

[24]Loftin, L. K., Jr. and von Doenhoff, A. E., "Exploratory Investigation at High and Low Subsonic Mach Numbers of Two Experimental 6-Percent Thick Airfoil Sections Designed to Have High Maximum Lift Coefficients," RM L51F06, 1951, NACA.

[25]Stratford, B. S., "The Prediction of Separation of the Turbulent Boundary Layer," *Journal of Fluid Mechanics*, Vol. 5, 1959, pp. 1-16.

[26]Schlichting, H., *Boundary-Layer Theory*, 6th ed. McGraw-Hill, New York, 1968.

[27]Liebeck, R. H., "A Class of Airfoils Designed for High Lift in Incompressible Flow," *Journal of Aircraft*, Vol. 10, Oct. 1973, p. 610-617.

[28]James, R. M., "A New Look at Two-Dimensional Incompressible Airfoil Theory," Rept. MDC J0918/01, May 1971, Douglas Aircraft Co., Long Beach, Calif. (restricted distribution).

[29]Gartshore, I. S., "Predictions of the Blowing Required to Suppress Separation from High Lift Airfoils," *CASI Transations*, Vol. 4, March 1971, p. 39.

[30]Stevens, W. A., Goradia, S. H., and Braden, J. A. "Mathematical Model for Two-Dimensional Multi-Component Airfoils in Viscous Flow," NASA Contractor Rept. CR-1843, July 1971, NASA.

[31]Stevens, W. A., Goradia, S. H., and Braden, J. A., "Mathematical Model for Two-Dimensional Multi-Component Airfoils in Viscous Flow," AIAA Paper 72-2, San Diego, Calif., 1972.

[32]Foster, D. N., Ashill, P. R., and Williams, B. R., "The Nature, Development and Effect of the Viscous Flow Around an Airfoil with High-Lift Devices," Tech. Rept. 72227, Jan. 1973, Royal Aircraft Establishment, Farnborough, England.

[33]Prandtl, L. and Tietjens, O. G., *Applied Hydro- and Aeromechanics*, Dover, New York, p. 155.

[34]Abbott, I. H., and von Doenhoff, A. E., *Theory of Wing Sections*, Dover, New York, 1958, p. 227.

[35]Perkins, C. D. and Hage, R. E., *Airplane Performance, Stability, and Control*, Wiley, New York, 1954, p. 78.

[36]Chen, A. W., "The Determination of the Geometries of Multiple-Element Airfoils Optimized for Maximum Lift Coefficient," TM-X-67591, 1971, NASA.

[37]Liebeck, R. H. and Smyth, D. N., "Study of Slat-Airfoil Combinations Using Computer Graphics," *Journal of Aircraft* , Vol. 10, April 1973, p. 254-256.

[38]Hess, J. L. and Smith, A. M. O., "Calculation of Potential Flow about Arbitrary Bodies," *Progress in Aeronautical Science*, Vol. 8, Pergamon Press, New York, 1966.

[39]Callaghan, J. G. and Beatty, T. D., "A Theoretical Method for the Analysis and Design of Multielement Airfoils," *Journal of Aircraft*, Vol. 9, Dec. 1972, p. 844-848.

[40]Gentry, A. E., "How Sails Work," *SAIL Magazine* (in several issues between April 1973 and Oct. 1973).

[41]Ashill, P. R., "A Study of the Effect of the Wake of the Main Aerofoil of a Fowler Flap Configuration on the Lift of the Flap," Tech. Rept. TR 72081, July 1972, Royal Aircraft Establishment, Farnborough, England.

[42]Moser, A. and Shollenberger, C. A., "Inviscid Wake-Airfoil Interaction on Multielement High Lift Systems," *Journal of Aircraft*, Vol. 10, Dec. 1972, p. 765-770.

[43]Wilkinson, D. H., "A Numerical Solution of the Analysis and Design Problems for the Flow Past One or More Aerofoils or Cascades," R&M 3545, 1967, Aeronautical Research Council, London.

[44]Cebeci, T. and Smith, A. M. O., *Analysis of Turbulent Boundary Layers*, Academic Press, New York, 1974.

[45]Cebeci, T. and Witherspoon, G. F., "Theoretical Suction and Pressure Distribution Bounds for Flow Separation in Retarded Flow," *Journal of Aircraft*, Vol. 11, Jan. 1974, pp. 61 -64.

[46]Gartshore, I. S. and Newman, B. G., "The Turbulent Wall Jet in an Arbitrary Pressure Gradient," *The Aeronautical Quarterly*, Feb. 1969, p. 25.

[47]Shen, C. C., Lopez, M. L., and Wasson, N. F., "A Jet-Wing Lifting-Surface Theory Using Elementary Vortex Distributions," *Journal of Aircraft*, Vol. 12, May 1975, pp. 448-456.

[48]Halsey, N. D., "Methods for the Design and Analysis of Jet-Flapped Airfoils," *Journal of Aircraft*, Sept. 1974, pp. 540-546.

[49]Nash, J. F. and Patel, V. C., *Three-Dimensional Turbulent Boundary Layers*, S. B. C. Tech. Books, Atlanta, Ga., 1972.

[50]Cebeci, T., "A General Method for Calculating Three-Dimensional Incompressible Laminar and Turbulent Boundary Layers; II. Three-Dimensional Flows in Cartesian Coordinates," Rept. MDC J6517, Mar. 1974, Douglas Aircraft Co., Long Beach, Calif.

[51]Kline, S. J., Morkovin, M. V., Sovran, G., and Cockrell, D. S., "Computation of Turbulent Boundary Layers," AFOSR-IFP-Stanford Conference, Stanford Univ. Press, 1968.

[52]Cornish, J. J., III, "High-Lift Applications of Spanwise Blowing," Paper No. 70-09, *Seventh Congress of the ICAS*, Rome, 1970.

[53]Krall, E. M., and Haight, C. H., "Wind Tunnel Tests of a Trapped-Vortex High-Lift Airfoil," Rept. B-94300/3TR-10, Advanced Technology Center, Dallas, Texas.